FEDERAL UNIVERSITY OF TECHNOLOGY OF PARANÁ /
UNIVERSITY OF APPLIED SCIENCES MANNHEIM
GRADUATE PROGRAM IN ELECTRICAL AND COMPUTER ENGINEERING

BRITTA ANGELA RÜLANDER

GALVANIC VESTIBULAR STIMULATOR FOR FMRI RESEARCH

DISSERTATION

CURITIBA / MANNHEIM

2016

BRITTA ANGELA RÜLANDER

GALVANIC VESTIBULAR STIMULATOR FOR FMRI RESEARCH

Dissertation presented to the Graduate Program in Electrical and Computer Engineering of the Federal University of Technology of Paraná / University of Applied Sciences Mannheim as a requirement for obtaining the title of Master of Science, M.Sc. – Concentration Area: Biomédica - Biomedical Engineering.

Supervisor: Prof. Dr. Humberto R. Gamba

Co-supervisor: Prof. Dr. Marcus Vetter

CURITIBA / MANNHEIM

2016

ACKNOWLEDGEMENT

This master thesis is based on the work, support and efforts of a lot of people and institutions to whom I want to give my many and genuine thanks.

To my supervisor Prof. Dr. Humberto R. Gamba for his support and guidance during the whole thesis, especially during the exchange year at UTFPR in Brazil; for his time and input on hours of testing, planning, developing and creating of ideas; without any hesitation to advise me.

To my co-supervisor Prof. Dr. Marcus Vetter for his advise and supervision of my master thesis on the German side.

To Tiago Manzcak for his initial help and ideas to enhance the underlying thesis.

To Felipe Gonzales and João Pedro Curti for their collaboration in the thesis, especially during the development of the PCBs and firmware.

To CAPES (Coordenação de Aperfeiçoamento de Pessoal de Nível Superior) for the financial support.

To my friends and family for their enormous support and consistent motivation to help this thesis becoming a reality.

ABSTRACT

RÜLANDER, Britta A.. GALVANIC VESTIBULAR STIMULATOR FOR FMRI RESEARCH. 90 f. Dissertation – Graduate Program in Electrical and Computer Engineering, Federal University of Technology of Paraná / University of Applied Sciences Mannheim. Curitiba / Mannheim, 2016.

This master thesis presents the further development of a galvanic vestibular stimulator for use in fMRI examinations developed in a previous thesis (MANCZAK, 2012). This thesis amends the GVS by circuits to measure feedback values and implements the stimulation circuit with digital components, such as a microcontroller and flyback integrated circuits. The microcontroller is used in order to control the current source and process the measured values. The communication between the PC, which allows user interaction through a graphical user interface, and the microcontroller is implemented through optical communication, which is defined by a communication protocol specification. The digital circuitry is designed to be placed within the MRI room, meeting the requirements imposed by strong magnetic fields and radio frequency pulses. The underlying hypothesis of the thesis is that the device can be placed within the MRI room without having a negative impact on the MRI image quality. Laboratory tests without the MRI confirmed the correct design of the galvanic vestibular stimulator.

Keywords: Galvanic vestibular stimulation; fMRI; optical transmission

LIST OF FIGURES

LIST OF TABLES

LIST OF ACRONYMS

fMRI	functional Magnetic Resonance Imaging
GVS	Galvanic Vestibular Stimulator
MRI	Magnetic Resonance Imaging
RF	Radio Frequency
BOLD	Blood Oxygen Level-Dependent
CVS	Caloric Vestibular Stimulation
EEG	Electroencephalogram
AC	Alternating Current
PGA	Programmable Gain Amplifier
IC	Integrated Circuit
DAC	Digital to Analogue Converter
MSP	mixed signal microcontroller family by Texas Instrument
EMI	Electromagnetic Interference
RFI	Radio Frequency Interference
ADC	Analogue to Digital Converter
CRC	Cyclic Redundancy Check
SFD	Start Frame Delimiter
UART	Universal Asynchronous Receiver Transmitter
rms	Root Mean Square
DMA	Direct Memory Access
GUI	Graphical User Interface

CONTENTS

1 INTRODUCTION

Vestibular stimulation has been of interest during the past years and thus bears the possibility of interesting research projects (JUSTINA, 2014) (MANCZAK, 2012) (DELLA-JUSTINA et al., 2015) (DELLA-JUSTINA et al., 2014). Galvanic stimulation is one of the main possibilities to stimulate the human vestibular system (WARDMAN et al., 2003) (MACDOUGALL et al., 2006) (AW et al., 2006), amongst other procedures such as caloric stimulation (FASOLD et al., 2002) (MARCELLI et al., 2009). But galvanic, or in other words electric, stimulation encounters challenges when being used in medical research utilizing functional magnetic resonance imaging further referred to as fMRI (fMRI). This master thesis builds on a previously developed galvanic vestibular stimulator (GVS) that is used to study the body balance system of healthy subjects, making it more safe and secure to be operated by any researcher interested in studying the human brain (MANCZAK, 2012). His thesis' protocol is basically being added to by a control unit, such as a microcontroller, and other digital devices in the project. A whole new version of the GVS is being developed to enable auto-regulation and the measurement of feedback values. This master thesis evaluates whether digital circuits used in an electronic stimulator can be used in fMRI without causing interference and information loss within the imaging. Furthermore, it will discuss whether it would even be possible to implement an electronic device without risking a compromise in image quality. The first chapter is comprised of the motivation as well as the general and particular objectives for starting and completing this master thesis. Then the technical foundations will be outlined in chapter 2. Chapter 3 will illustrate the methods and materials used within this thesis and the results and their discussion are presented in chapter 4. The conclusion is then depicted in chapter 5. Finally, the thesis terminates with a prospect to further developments in chapter 6.

1.1 MOTIVATION

Being able to maintain balance seems to be nothing but normal. Still a lot of people suffer from dizziness and vertigo in normal situations. Although it is known that this may be caused by various diseases, there are still many doubts about how to best diagnose and treat these conditions (GUINAND et al., 2015) (KERBER; NEWMAN-TOKER, 2015). One aspect to help in those situations is to outline the specific areas of the brain that process the input information and control the equivalent reaction to retain the equilibrium. One idea is that it may

be possible to stimulate the corresponding brain areas, causing them to perform their normal function if these brain areas themselves cannot guarantee the body balance. Thus it is important to detect the exact brain regions responsible for the information processing. Using the fMRI, targeted vestibular stimulation may outline the brain areas and help to determine exact brain stimulation points. It is known that visual and vestibular systems work together in order to support the static body equilibrium. In a recent publication that demonstrates the potential of this field of research, the interacting areas of the brain that are responsible for the vestibular and visual system were mapped for non-symptomatic subjects. Visual and electrical vestibular stimulation was applied in fMRI experiments (JUSTINA, 2014). A detailed description of the galvanic stimulator used in these experiments can be found elsewhere (MANCZAK, 2012).

1.2 GENERAL OBJECTIVES

One of the main objectives of this master thesis is the development of a medical device that can be properly used within the magnetic room of a magnetic resonance imaging (MRI) system. In order to both ensure the patient's safety as well as the flawless functionality and outcome of the imaging some main characteristics must be guaranteed. Besides the security regulations and requirements, enforced by law, the correct functionality of the MRI system is implied by obvious reasons like the fMRI's usability. If the results turned out to be incorrect or uncontrolled, they would be unable to be used for research purposes as they could neither be used to confirm nor refuse the thesis, nor would they be repeatable. The development objectives of such a device can be separated into purely practical and developmental purposes and measuring or controlling units. The first development stage is to guarantee the device's functionality before appending the control units which add more regulations and restrictions to the project. A brief overview of the thesis' development looks as follows:

- Define the requirements and limitations for a proper galvanic vestibular stimulator.
- Design a circuitry for the stimulation and measurement of the galvanic vestibular stimulator.
- Build the electronic circuit.
- Define the communication protocol for software and firmware.
- Divide the functionality of the stimulator between the microcontroller and the computer.
- Implement the firmware and software.

- Laboratory tests with the whole system and software, firmware and hardware installation.
- Project and construction of a Faraday shield box.
- Tests within an MRI.

Furthermore, some specific objectives can be named that are more development related and constitute new attempts to implement other circuitry possibilities. These specific objectives are outlined in subsection 1.2.1.

1.2.1 SPECIFIC OBJECTIVES

Besides the medical research interest in mapping the brain areas that are related with the body balance system, there is also a strong technological interest in gaining experience in developing dedicated electronic devices for MRI. The specific technological requirements that are imposed by the MRI environment (strong magnetic field, radio frequency pulses (RF pulses), magnetic gradients) present a non-trivial challenge to be overcome. Especially considering an electronic device, placed near to the subjects feet, that has a pair of electrical wires going through the magnetic bore and that connect to a pair of electrodes placed over the mastoid process of a subject. The medical application adds another difficulty to the design of the device as the safety of the patient has to be ensured.

In comparison to the first prototype of the GVS, digital components are integrated into the circuit to prove the hypothesis that, if the circuit is well shielded, it will not interfere with the MRI system and vice-versa. Adding a microcontroller to the device will improve the controlling and information processing and allow some sort of auto-regulation and feedback. The GVS functionality will also improve in terms of usability and simplicity to operate; making it easy to use the device in medical research projects. The main hypothesis of this thesis is, that if the digital circuitry is well enclosed in a Faraday shield it will not influence the MRI image quality in such a negative way that the device would risk the outcome of the imaging and therefore could not be used; but that it even permits a more practical functionality.

2 TECHNICAL FOUNDATION

Having outlined the motivation and objectives of this master thesis, this chapter presents the technical and physiological foundations and gives a representative selection of literature related to galvanic and non-galvanic vestibular stimulation. This chapter is meant to indicate physiological and technical basics for further insight into the thesis' presuppositions and demands. First of all the physiological structure of the human vestibular system is outlined. Then the fundamentals of MRI and galvanic stimulation are broached and last of all some significant articles and papers are being put forward.

2.1 VESTIBULAR SYSTEM

This first section will depict the physiology of the human vestibular system and its functionality before outlining the technical foundations of the galvanic vestibular stimulation.

The human balance is a complex system, which is composed of various functional units of the human body. To retain equilibrium the vestibular system collaborates with the visual and somatosensory systems. The brain comprises all the information obtained and evaluates what actions to take in order to guarantee balance. In contrast to visual and somatosensory inputs from muscles and joints which are obvious and comprehensible, the vestibular system and its contribution to balance is more complex. The vision senses the relative orientation towards the surroundings, and somatosensory information outlines the muscle and joint position and contraction whereas the vestibular system provides information about spatial orientation and motion as well as its direction and equilibrium. The vestibular system is situated in the inner ear.

Figure 1 shows the illustration of the human inner ear. It consists of the cochlea, the main auditory organ, and the vestibular system. The vestibular system can be divided into five distinct organs, the three semicircular canals and two otolith organs. Within this division the semicircular canals are sensitive to angular accelerations which occur during head rotations while the otolith organs detect the linear accelerations and sense the head position. The three semicircular canals are mutually orthogonal and can thus distinguish and specify the direction and acceleration of any head rotation. There are three planes of rotation which are commonly referred to as pitch (up and down), roll (tumbling from left shoulder to right and vice versa) and

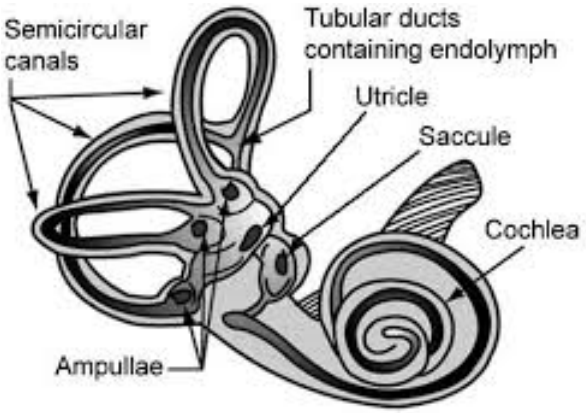

Figure 1: Figure of the human inner ear including the vestibular system and the cochlea.
Source: Human Vestibular System in Space. (NASA, 2004)

yaw (lateral movement to the left and right). Each semicircular canal is situated in one plane and is specialized and maximally responsive to angular motion within this distinctive plane. The semicircular canals are differentiated as horizontal, anterior and posterior canal. The otolith organs are distinguished as utricle and saccule. They have distinctive sensing characteristics as the utricle detects motion in the horizontal plane and the saccule senses motion in the sagittal plane.

The underlying principle of vestibular sensing is based on Newton's first law of motion, often referred to as Law of Inertia. This law states: 'Every body persists in its state of rest or of moving uniformly straight forward, except insofar as it is compelled to change its state by force impressed.' The law can often be experienced as a delay in fluid motion. In the human vestibular system the Law of Inertia comes into action because the semicircular canals are filled with a fluid called endolymph. When the body starts moving or rotating, all parts connected to the body (like bone and soft tissue) move simultaneously. The endolymph then lags behind because of inertia. It applies pressure on the sensory receptors of the canals through its movement. These sensors are called hair cells.

This fluid mechanically bends the hair cell's cilia so that the tip link is stretched and potassium ions enter the cell. The potassium influx generates a neural impulse which is sent to the brain via VIIIth cranial nerve. The tallest cilium is called the kinocilium (see figure 2). A cilium bending towards the kinocilium depolarizes the cell and the afferent activity is increased. A bending away from the kinocilium hyperpolarizes the cell and the afferent activity is decreased.

The processing and integration of the sensory input takes place in the brain, in which

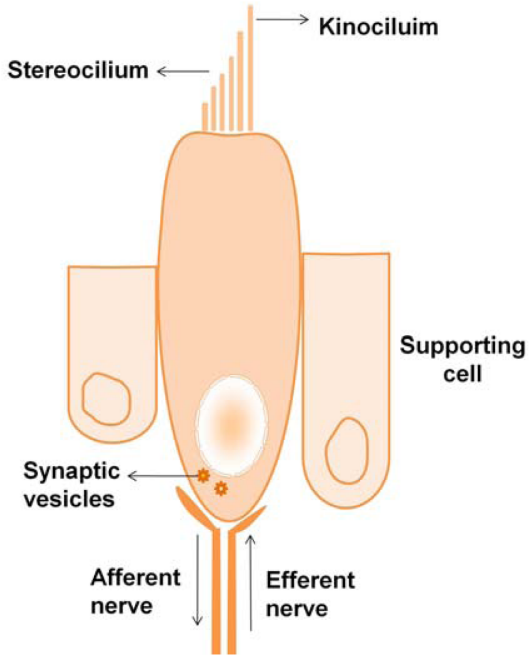

Figure 2: Figure of a typical hair cell from the vestibular system.
Source: Journal of Functional Biomaterials, 2011, 2.

the cerebellum acts as the coordination center to initiate automatic movements and the cerebrum acts as the thinking and memory center which retrieves previously learnt information. The vestibular system interacts with the visual system in a way that it is able to control eye movements according to the sensory vestibular input. Thereby the vestibular system contributes to more than just balance and might help to maintain the focus for example in trained spinning movements like ballet pirouettes.

Since the human balance system is a complex and interconnected system, the diagnosis and treatment of balance dysfunctions are relatively complicated. One aim of research is to concentrate on the different functional units and assess their position and contribution to the balance more precisely.

2.1.1 GALVANIC STIMULATION OF THE VESTIBULAR SYSTEM

After having depicted the physiological characteristics of the human vestibular system, this subsection presents the basic physiological principles for the success of galvanic vestibular stimulation of the human vestibular system. The application of a small galvanic current to induce transcutaneous electrical nerve stimulation has been presented in various research publications such as Fitzpatrick and Day (2004) and Della Justina (2014).

The galvanic current is applied to the afferent vestibular nerves which are located close

to the mastoid bone right behind the ear on both sides of the head. GVS is often executed as bipolar bilateral stimulation, meaning that the electrical cathode is placed behind one ear and the electrical anode behind the other. The electrodes are placed on the head surface above the mastoid bone. The galvanic stimulus itself is generated by a current source which is controlled by the researcher, later referred to as user. Fitzpatrick and Day (2004) stated that an efficient current configuration is given through an amplitude of 1 mA, a frequency of 1 Hz and a wave form equal to a sine wave.

It is shown that GVS affects the cell membrane potential of the semicircular canals in the same way ipsilateral or contralateral acceleration does but that it does not evoke a sensation of acceleration towards one specific direction like natural vestibular stimulation would. The GVS causes the ciliar cells to align which induces a change in the electric potential of the afferent nerves that innervate the ciliar cells. An explanation for GVS stimulating the vestibular system is given by Fitzpatrick and Day (2004).

Having been outlined in section 2.1, the afferent fibers depolarize and the firing rate increases when the stereocilia deflect towards the kinocilium. If they deflect in the opposite direction, the afferent fibers hyperpolarize and the firing rate decreases. During GVS the firing rate is always increased on the side of the head where the cathode is placed on the mastoid bone. A horizontal and an ipsilateral rotation, referred to as yaw and roll, is experienced by the patient. On the other side of the head, where the anode is placed above the mastoid bone, the firing rate of the afferent fibers always decreases. Summarizing this, cathodal and anodal stimulation cause a sensation of rotation in opposite directions.

Further it has been shown in Fitzpatrick and Day (2004) that cathodal stimulation also increases the firing rate of the utricle afferent fibers. This is the same response which normally indicates an acceleration in direction of the cathode. On the contralateral side the anodal stimulation results in a smaller disequilibrium of the cilio cell alignment which indicates an acceleration in direction of the anode. Summing up, the stimulation results in the sensation of a small acceleration towards the cathode given by the utricle afferent fibers.

Altogether, GVS can cause the impression of both linear acceleration towards the cathode electrode and inclination toward the anode electrode.

2.2 MAGNETIC RESONANCE IMAGING

Multiple medical sections use MR imaging such as for brain examinations and tumor diagnosis. In order to understand the characteristics and technical foundations of fMRI, the

principles of MR imaging are outlined in 2.2.1. After that, the special features of fMRI are shown in 2.2.2.

2.2.1 MRI

Magnetic resonance imaging marks itself being a non-invasive imaging technique which is especially used to demonstrate morphology and tissue structures with high resolution in time and space. The main advantage of MRI is that it does not utilize ionizing radiation and thus it is classified to be safe for the patient (SOLUTIONS, 2003). The MRI technique is based on the nuclear spin of hydrogen atoms. This nuclear spin has magnetic characteristics and can be externally deflected by a magnetic field. It refers to the hydrogen atom because of its basic structure of the nucleus, consisting of one proton only. Furthermore, hydrogen is the most common atom within the human body as it is the main part of both water and fat. Thus its spin generates the most intense signal. The interaction of nuclear spins within tissue is specific and generates a characteristic signal which can be processed to create the image (SOLUTIONS, 2003). This chapter describes the technical and physical foundation of MRI.

As already mentioned, the nuclear spin is a quantum mechanical characteristic of particles. It can be described as rotation around its own axis which never stops. A nuclear spin only exists in atoms with an odd number of protons and neutrons such as hydrogen. The nuclear spin is linked to a magnetic force and thus the nuclei of atoms are magnetized. The spins would compensate one another in a field-free environment as they are randomly aligned in space. The resulting total magnetization in this case would be zero. When applying an external magnetic field, the spins align with the magnetic field, almost equally parallel and antiparallel. The MRI technique does not consider each and every spin but focuses on the resulting total magnetization. Therefore the excess of spins aligning in one direction rather than the other generates the resulting total magnetization, as parallel and antiparallel aligned spins compensate each other. The preferred direction for alignment is parallel to the applied external field (SOLUTIONS, 2003) (See figure 3).

The alignment of the nuclear spins depends on their energy level. It has been proven that antiparallel aligned nuclear spins are on a higher energy level than parallel aligned nuclear spins (SOLUTIONS, 2003). When an external magnetic field is then used to align the nuclear spins, they start to precess around the axis that they are aligned to. The precession frequency is dependent on the formation of the nucleus and the strength of the external magnetic field. It is called Larmor frequency and is approximately 63 MHz for hydrogen and 1.5 T. The radio frequency coils are tuned so that they deflect the nuclear spins when applying a RF-pulse.

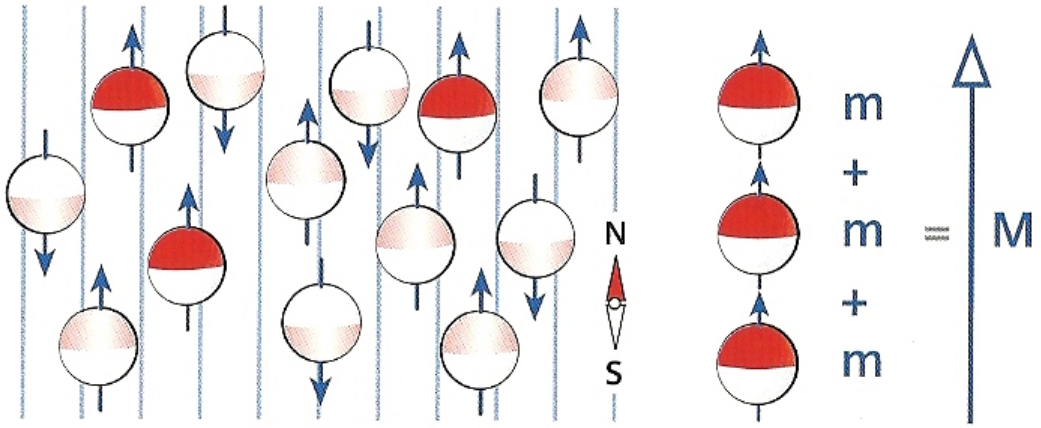

Figure 3: Figure of the resulting total magnetization.

Source: SIEMENS medical, 2003, p.34

Applying a 180° pulse overturns the nuclear spins within the z-dimension and shifts them into a state that is weaker than the prior one so that the nuclear spins try to realign. Therefore the longitudinal magnetization disintegrates again. A 90° pulse tilts the nuclear spins into the xy-plane which revokes the prior differences in phase. This process is called transversal magnetization. During the relaxation both longitudinal and transversal magnetization relapse, but with a different time constant T1 and T2 (WEISHAUPT et al., 2009).

The precession of the transversal magnetization induces an electrical voltage that can be measured over time. This measurement provides the MRI signal. The correlation between transversal magnetization and MRI signal is proportional. Thus, the sum of all nuclear spin resonances produces the MRI signal. This raw signal does not yet involve any spatial resolution. To be able to assign pixel information to spatial resolution, a gradient is applied along the magnetic field so that the magnetic field varies in one dimension. Due to the correlation between the intensity of the external magnetic field and the Larmor frequency of the nuclear spins, a slice selection can be induced by the applied gradient. Because of this only the spins within a specific slice are tilted by the pulse frequency into the xy-plane. Hereby the correlation between the gradient intensity of the magnetic field and the thickness of the selected slice is anti-proportional. When applying one gradient per dimension a fully spatial resolution can be guaranteed by frequency and phase coding. The raw data is placed in a matrix called k-space. Conducting a two-dimensional Fourier-transformation generates the MRI images. A three-dimensional picture can be generated by applying yet another gradient for phase coding in the z-direction to obtain further information on spatial volume(WEISHAUPT et al., 2009). The different sequences of operating the gradients are explained in other technical literature to

more extent.

2.2.2 fMRI

fMRI is a specific kind of MRI that tries to point out the neurological function of the brain. In order to measure the activity of neurons fMRI uses flow of oxygenated blood. It especially makes use of blood oxygen level-dependent, BOLD, contrast sequences for measurements of the human brain related to neurological activity that is regionally bounded. BOLD contrast is based on the paramagnetic characteristics of deoxyhemoglobin. It results from oxyhemoglobin, which is normally diamagnetic. The oxyhemoglobin renders the oxygen to the surrounding cells and tissue and becomes deoxygenated. The changing magnetic characteristics of oxy- and deoxyhemoglobin not only affect the MRI signal of the water molecules but even the molecules of the surrounding tissue through the vessel walls. The growing number of nuclear spins, that are affected by the paramagnetic deoxyhemoglobin, results in a form of amplification. The affected voxel appears dark in the image. Because BOLD contrast depends on the level of blood oxygenation, it is possible to measure all physiological events which result in a change of oxygenation (OGAWA et al., 1990).

One of the main advantages of fMRI is that it does not need any injection of signal-boosting compounds. The technique shows the blood flow to activated regions and generates signals from a greater depth and with a higher spatial resolution than other methods like EEG do. Due to this it is non-invasive and increasingly becomes the method of choice in brain science. Still, fMRI cannot measure the real neuronal activity because it does not give details about how many neurons are firing and is not able to distinguish whether the activation of these neurons dampens or amplifies the activity in the surrounding areas. The measured signal itself is the boost in flow of oxygenated blood in response to an applied stimulus. It is small and in consequence the signal-to-noise ratio is relatively low. There are approaches to boost the signal by using stronger magnets (i.e. seven or more Tesla). The assumption for why the oxygen carried in blood by hemoglobin increases after a stimulus is that it deflects the greater demand of oxygen that arises when the neurons are electrically activated (SMITH, 2012).

2.3 LITERATURE REVIEW: GALVANIC VESTIBULAR STIMULATION

Galvanic vestibular stimulation is a medical research topic which has been focused on for the last 25 years, if not even more. The fundamentals have already been laid by scientists as famous as Luigi Galvani and Count Alessandro Volta (COHEN et al., 2012). The first GVS

with fMRI did not took place before 1998 because research in technology reached its limits when trying to put an electronic device such as the galvanic vestibular stimulator inside the magnetic resonance room. The risks for the patient by induced currents would be too high and the interference with the magnetic resonance imaging too strong. There simply did not seem to be a way to make the fMRI exam possible (LOBEL et al., 1998). Before this, the exploration of the human brain was being conducted with caloric vestibular stimulation, CVS, or with help of electro-physiological potentials such as electroencephalogram (EEG). CVS is a technique where the external ear canal is irrigated with cold or warm water. This is able to identify areas of the human brain that correlate to the human vestibular system (LOBEL et al., 1998).

Nowadays GVS is an established method that is used in fMRI and is considered a simple and safe as well as a specific form of stimulation to examine the human vestibular system (FITZPATRICK; DAY, 2004). Both monopolar and bipolar galvanic stimulation are possible thus mostly bilateral, bipolar stimulation is used today. A galvanic stimulation utilizing AC current is proven to have some advantages over galvanic stimulation with DC current (STEPHAN et al., 2009). One advantage which is named here is that the DC stimulation only generates a vestibular sensation during on- and off-set of the DC stimulus while it is much weaker during the constant stimulation. On the contrary AC stimulation causes the patient to experience strong vestibular sensations for the duration of the whole stimulation period. Lobel et al. present GVS as a technique with a fast reaction time in contrast to CVS (LOBEL et al., 1998). New physiological findings allow the pursuit of GVS as they provide new information. Lobel et al. challenge the requirements by generating the stimulus waveforms with function generators and feeding the stimulus via optocouplers to the low pass LC filter. These are tuned to the Lamor frequency to prevent the pickup of radio frequency pulses and further on to twisted leads of carbon electrodes (LOBEL et al., 1998). With this technique GVS is made safe for the patient.

GVS equally stimulates the otolith organs and the semicircular canals and is thus an ideal technique to investigate the processing of vestibular information which is not hierarchically organized as a sensory procession in the brain. It has been shown that the areas processing vestibular stimuli also correlate with visual and somatosensory inputs. GVS is an important and very actual topic since 'Knowledge of the cortical areas involved in the processing of vestibular information is important because of the fundamental role of the vestibular system in motion perception, body orientation, eye movement and posture control' [Lobel et al., 1998, The American Physiologicl Society, p.2699, chapter: Introduction].

2.3.1 STIMULATION SEQUENCE

Having presented a short literature review about galvanic vestibular stimulation, this subsection points out possible stimulation sequences which can be used for fMRI exams utilizing GVS. A short description of the sequence is provided for better understanding of design requirements, especially of software and firmware. Stephan et al. (2009) highlights the advantages of AC current stimulation in GVS. Literature suggests an alternating sequence of stimulation and rest during the fMRI exam (STEPHAN et al., 2009). Most research reports the utilization of sinusoidal currents. However, triangular and quadrangular wave forms are also possible (STEPHAN et al., 2009). The general idea is to enable a stimulation sequence that alternates between these different waveforms and a rest phase for varying periods of time. The number of repetitions both of each stimulus and the whole sequence can be adjusted according to research purposes. An fMRI exam with GVS takes about forty minutes and might contain various alternations of current and rest, depending on the experimental setup. As this thesis only claims to be technological and not medical, it does not focus on the different sequences that achieve diverse research aims. The implementation of the stimulation is shown in section 3.5 respectively subsection 3.3.4.

3 MATERIALS AND METHODS

This chapter outlines the design and development of hardware, firmware as well as software. The main parts of the development steps are depicted. The development process can be divided into the following sections which present a development overview in section 3.1, the stimulation circuit design in section 3.2, the control circuit design in section 3.3, the security circuit design in section 3.4 and the software development in section 3.5.

3.1 DEVELOPMENT OVERVIEW

As already outlined before, this master thesis is based on a previous thesis (MANCZAK, 2012). This newer version aims at modifying the structure of the hardware and adding supplementing components to the design as well as amending the software and firmware with new functionalities.

The hardware development must meet some requirements and stimulation characteristics which has been determined through former tests and research (MANCZAK, 2012) (JUSTINA, 2014) (STEPHAN et al., 2009). The desired stimulation characteristics are shown in table 1.

Wave form	Frequency	Amplitude
sine	1 Hz	0.5 mA_p
quadrangular	1.5 Hz	1 mA_p
triangular	2 Hz	1.5 mA_p
-	2.5 Hz	2 mA_p
-	3 Hz	2.5 mA_p
-	3.5 Hz	3 mA_p
-	4 Hz	3.5 mA_p
-	4.5 Hz	4 mA_p

Table 1: Desired stimulus characteristics for wave form, frequency and amplitude of the applied current.

Source: Own authorship

The desired characteristics, especially the peak amplitude, determine the design characteristics of the current source used in this thesis as the current output of the current source

defines the required voltage input und voltage supply. Further details are outlined in section 3.2.

The first step is to establish a new hardware design, containing the selected microcontroller for the control circuit and another way to build a current source for galvanic stimulation. The selection of the new components, such as the microcontroller and the components for the current source (programmable gain amplifiers (PGA) and flyback IC as explained in subsection 3.2.2) forms a big part during the first development task.

Afterwards the communication protocol is designed to guarantee a flawless interaction between firmware and software. These two programs are almost independent and just interact through the communication interface. The firmware and software can thus be developed parallel to each other, after defining their main characteristics and structure.

The design of a user interface faces both programming challenges and design tasks. Many tests are part of the development process before having a satisfying working and interface solution.

Before explaining the development steps in detail, subsection 3.1.1 gives an overview of the project development with the help of different block diagrams.

3.1.1 BLOCK DIAGRAM

The project structure can be simplified and represented as a block diagram depicting the different sections of the project development. Certainly it only provides an overview as a detailed description and presentation is given in the following sections. Figure 4 shows the block diagram of the whole GVS project.

Generally speaking the project structure can be divided into two parts: the development of hardware and software for the control room on one side and the development of hardware and firmware for the MRI room on the other side. Since the detailed project description following in the subsequent sections presents the underlying project development characteristics and a more profound insight, the block diagram shown here only depicts the fundamental ideas and structure.

The requirements in respect to the section being placed in the control room are not as challenging as for the section being placed in the MRI room. It basically consists of two units: the PC for user interaction and a hardware part for the implementation of the communication with the hardware in the MRI room. The hardware board implements four main functionalities: the reception of the MRI trigger for synchronization of the GVS with the MRI device, the connection to the PC via USB adapter and the implementation of the optical communication

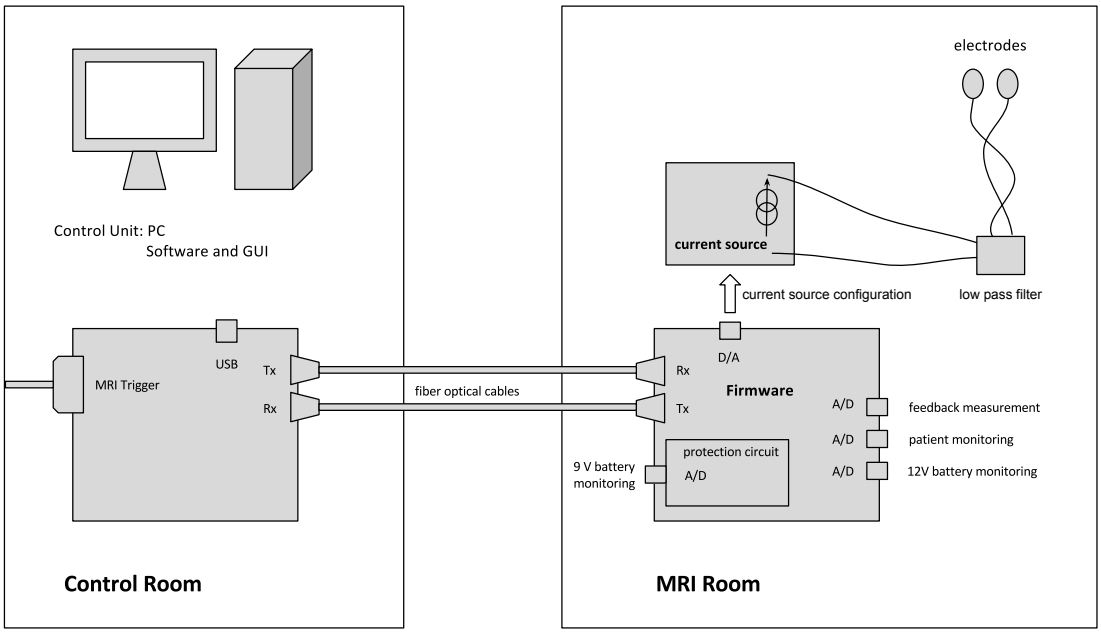

Figure 4: Simplified representation of the project structure in the form of a block diagram. The different sections of the GVS project are depicted as a slight overview of the project design.
Source: Own authorship

canal for the communication between the two hardware boards.

The design and implementation of the hardware for the MRI room is more challenging as multiple design requirements must be met to guarantee minimal imaging interference and to avoid magnetic and radio frequency interference for the circuitry itself. The hardware implements the main characteristics. This includes the current source, the feedback measurement, battery and patient monitoring, the whole protection circuit and finally the counterpart in optical communication. The electrodes are a simplified representation for the current application. The second part, the design and development of the firmware, implements the data processing, the communication protocol and the current source control.

The development of software, firmware and all hardware parts is depicted in detail in the following sections and subsections.

The hardware development is further depicted in the two following figures 5 and 6. Figure 5 provides a general overview of the current source circuit, including voltage supply circuitry and the signal conditioning. The ICs used for specialized functions are determined in the block diagram to provide a more detailed information about the circuits. However,

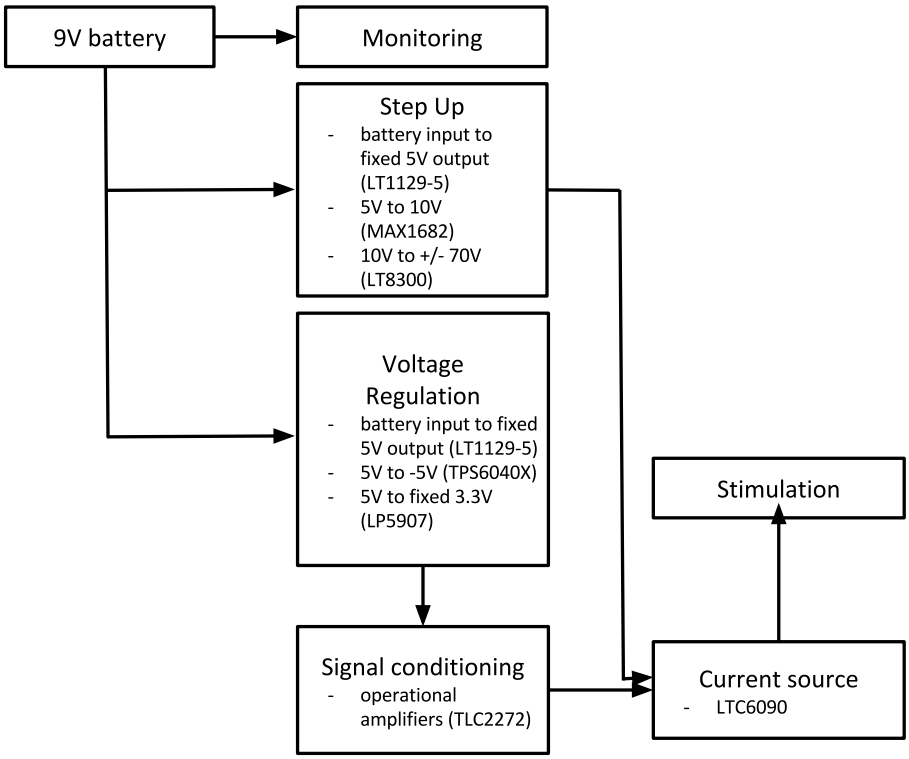

Figure 5: Hardware block diagram of the current source structure providing information about the ICs used in this project section.

Source: Own authorship

the operational amplifiers for amplification or measurement purposes are not specified in the diagram and will be described later.

The current source circuit structure includes two main functions: the monitoring of the battery level for security purposes and the current generation and conditioning. Step up circuitry and voltage regulation only serve the goal to provide the appropriate voltage supply for the different ICs used in the hardware section. The signal conditioning part ensures the proper input for the current source which then furnishes the stimulation current to be applied to the patient.

The protection circuit structure is also straight forward. Figure 6 presents a simplified block diagram. It gives an overview of the structure and the different blocks contained in the protection circuit. The voltage supply is given by the 9V battery that is monitored for security purposes. The voltage regulation again provides the adequate voltage levels for the different ICs in this circuit. As indicated by the name the main function of this circuit is the patient protection and safety. Thus the three main parts of the circuit are the feedback measurement,

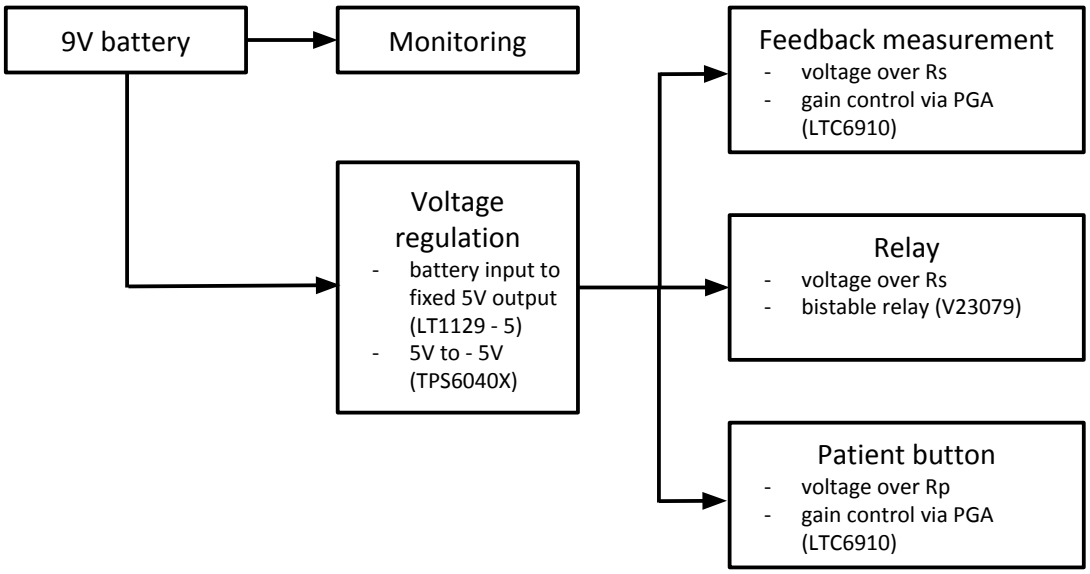

Figure 6: Hardware block diagram of the protection circuit structure depicting the ICs used in this project section. R_s is the designator of the shunt resistor placed in series with the patient to monitor the electrical current. The relay is used to protect the subject in case of an overcurrent. The patient button is a customised nylon structure which is placed over the subjects belly. The inner button structure consists of a normal open push button that is kept pressed by the subjects hand. By removing this pressure the electrical current bypasses the subject and the stimulation is interrupted.

Source: Own authorship

the monitoring of the patient button and the implementation of the overcurrent relay. The special ICs used in this project section are depicted in the block diagram.

The following sections of this chapter now focus on the detailed design and development steps.

3.2 STIMULATION CIRCUIT DESIGN

The stimulation circuit constitutes the main part of the project. It provides an important functionality and enables the stimulation itself. This section outlines concisely the design and implementation of the stimulation circuit and explains the application of the GVS.

In a previous study it has been shown that the impedance between the electrodes placed on the mastoid processes is approximately 15 kΩ and that the current source must provide an

adjustable electrical peak current of approximately 0.5 mA to 4.5 mA (MANCZAK, 2012). Thus, it is necessary to supply the current source with at least +-67.5 V_{pp}. Subsection 3.2.1 describes the current source circuit of a Howland current pump. The basic concept of the current generation is outlined with the help of the equation the circuit is based on. Subsection 3.2.2 provides an overview of the current source supply. It outlines the elevation of the voltage level from 9 V input to approximately +/- 75 V. Eventually, the last subsection 3.2.3 presents the output filters that were designed to prevent the MRI RF pulses and gradients to induce electrical current in the connecting wires which would interfere in the current source functionality or even destroy the circuitry.

The following sections outline the whole process of generating the current to be applied to the patient, beginning with the voltage supply and the multiplication by step up converters and ending with the signal which enters the electrodes.

3.2.1 CURRENT SOURCE

The design of the current source used in this project is based on the so called Howland current pump. A study of the Howland current pump (PEASE, 2008) outlines the design characteristics and explains the general function of the circuit. Figure 7 presents a basic Howland current pump. With $R_1 = R_3$, $R_2 = R_4$ and $R_5 = R_6$ follows:

$$I_L = -\frac{V_1 * R_2}{R_1 * R_6}$$

Thus, the load current is controlled by the voltage input and the resistor ratio of $\frac{R_2}{R_1}$. The resistor R_6 represents the sensitivity of the circuit. If R_6 is configured to be small in relation to the load resistance, the voltage across R_5 and R_6 can be diminished. The output resistance is calculated as follows:

$$R_{out} = \frac{R_1 * R_6 * (R_3 R_4)}{R_3 * (R_2 + R_5) - R_1 * (R_4 + R_6)}$$

For $R_1 = R_3$, $R_2 = R_4$ and $R_5 = R_6$ follows a R_{out} approximating ∞, which is desired for an electrical current source since it thus guarantees a constant current output for any load resistance.

In this thesis, the operational amplifier used for the current source is a LTC6090 provided by Linear Technology (LINEAR TECHNOLOGIES, 2012b). It is a current operational amplifier with 140 V CMOS rail-to-rail output and picoamp input and is supplied with +70 V and -70 V.

The current source is driven by the microcontroller which configures the digital to

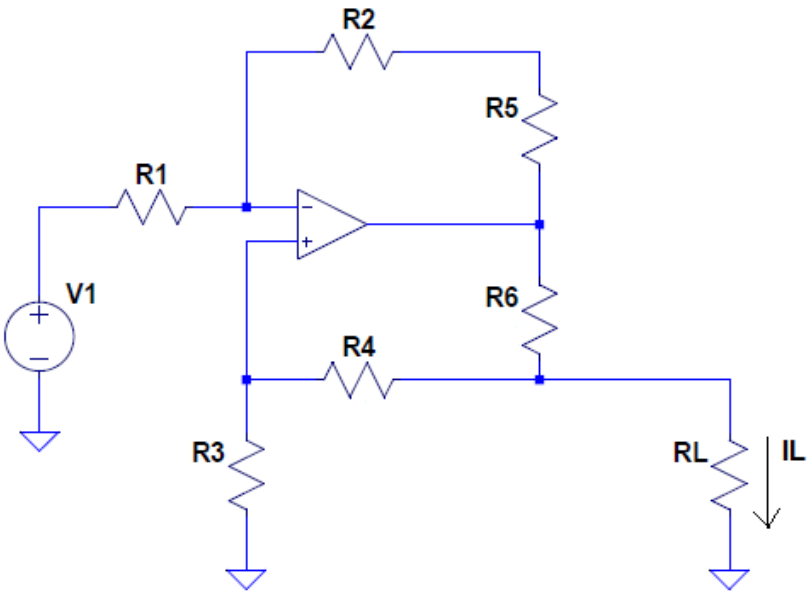

Figure 7: Basic design of a Howland current pump.

Source: (PEASE, 2008)

analogue converter (DAC) output according to the configuration done by the user. Its output signal is further conditioned before driving the actual current source. Operational amplifiers conduct the signal conditioning. The operational amplifiers used here are advanced linear CMOS rail-to-rail operational amplifiers with the designator TLC2272 provided by Texas Instruments Incorporated (TEXAS INSTRUMENTS INCORPORATED, 2004). As the DAC output ranges approximately between 0 V and 3.3 V, which is the supply voltage of the microcontroller, the output signal is thus clamped to the median voltage in case of symmetrical waveforms such as sine waves. Thus, the signal conditioning basically aligns the signal symmetrically around 0 V.

Figure 8 presents an excerpt of the stimulation circuit including the actual current operational amplifier.

The conditioned signal provides the negative input. The output is returned to both positive and negative input. The current source provides the stimulation current in the range of 0 mA and 4.5 mA. The patient constitutes this load of the current source and transforms the voltage with an amplitude in V into a current with an amplitude in mA.

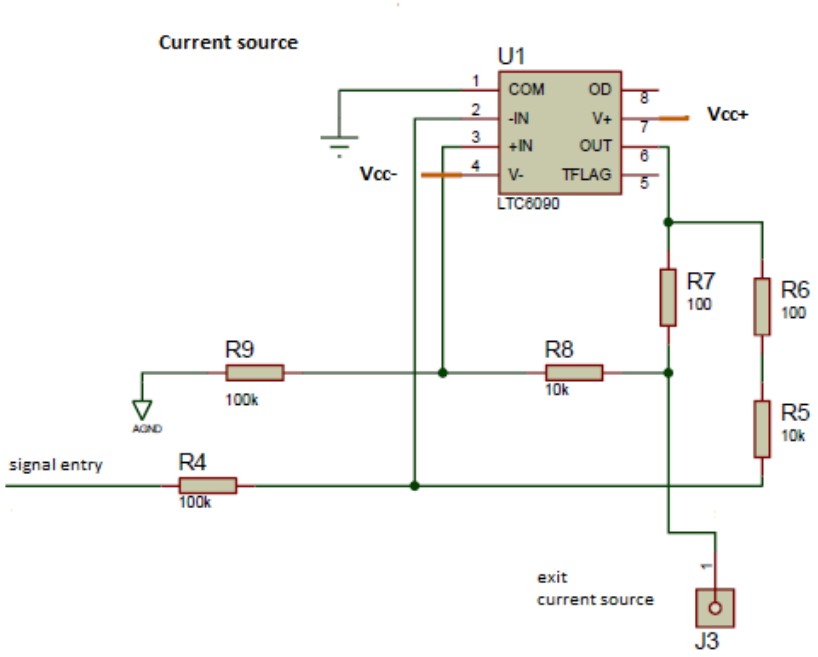

Figure 8: Excerpt from the stimulation circuit schematic showing the current source IC and the surrounding circuitry. Jumper 3 (J3) is the current source output. The load resistance is ground connected.

Source: Own authorship

3.2.2 CURRENT SOURCE SUPPLY

The voltage supply is provided by a 9 V battery. This voltage is converted to a fixed 5 V output by a micropower low dropout regulator with shutdown, specified by component number LT1129-5 by Linear Technology (LINEAR TECHNOLOGIES, 1994). The IC generates a fixed 5 V output from the varying input voltage provided by the battery. The battery voltage might hereby vary between 9 V to 55 V for the IC to be able to provide a 5 V output. Two LT1129-5 are used in the current source, one to supply the flyback circuit through a voltage multiplier (MAX1682) and one for the general voltage regulation that supplies the operation amplifiers.

For the voltage multiplication, the fixed 5 V output enters the next IC to step up to a voltage of 10 V. The IC is specified as a switched capacitor voltage doubler by Maxim Integrated Products, with part number MAX1682 (MAXIM INTEGRATED PRODUCTS, 2010). The MAX1682 offers a high voltage-conversion efficiency and only requires low operating currents. Two diodes lower the voltage to approximately 8.6 V which constitutes the input voltage for a micropower high voltage isolated flyback converter provided by Linear Technology, having the part number LT8300 (LINEAR TECHNOLOGIES, 2012a). The flyback IC generates the +70 V and -70 V output voltage, providing the supply voltage needed for the current source.

The flyback converter referred to before is designed for medical power supplies amongst other things. The micropower high voltage isolated flyback converter utilized in this project uses one unique flyback sense circuit and a sample-and-hold error amplifier to regulate the isolated output voltage from the flyback pulse. Generally speaking, the flyback voltage is converted to a current by the flyback pulse sense circuit. This current is amplified through the transformer turns ratio and through combination of other parameters and results in a magnified voltage providing both V_{out}+ and V_{out}-. Figure 9 presents an excerpt from the current source schematic depicting the circuitry involving the isolated flyback converter. The design and dimensioning of the circuitry integrating the isolated flyback converter pursues the example given in the LT8300 data sheet.

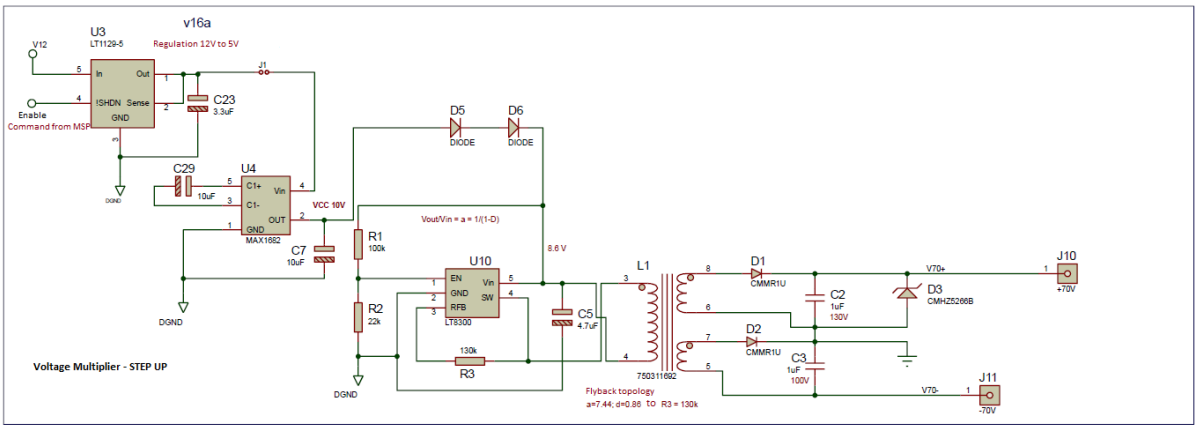

Figure 9: Excerpt from the stimulation circuit schematic presenting the isolated flyback converter and the surrounding circuitry.

Source: Own authorship

The voltage output is programmed by just one external resistor, here designated as R3 and dimensioned as 130 kΩ.

3.2.3 CURRENT SOURCE OUTPUT FILTERS

The two 600 W surface mount transient voltage suppressor diodes of the type SMBJ85CA-13 provided by Diodes Incorporated (DIODES INCORPORATED, 2009) are connected between GND and each wire leading to the electrodes. They protect the circuit against electrostatic discharges which might damage the connected circuitry.

The current source is the center of the stimulation circuit. It provides the main functionality of this master thesis. The circuitry can be divided into five sections, each having a different focus to contribute to the current generation.

Figure 10 presents an excerpt from the detailed stimulation circuit showing the

connection to the two electrodes which apply the desired current to the patient.

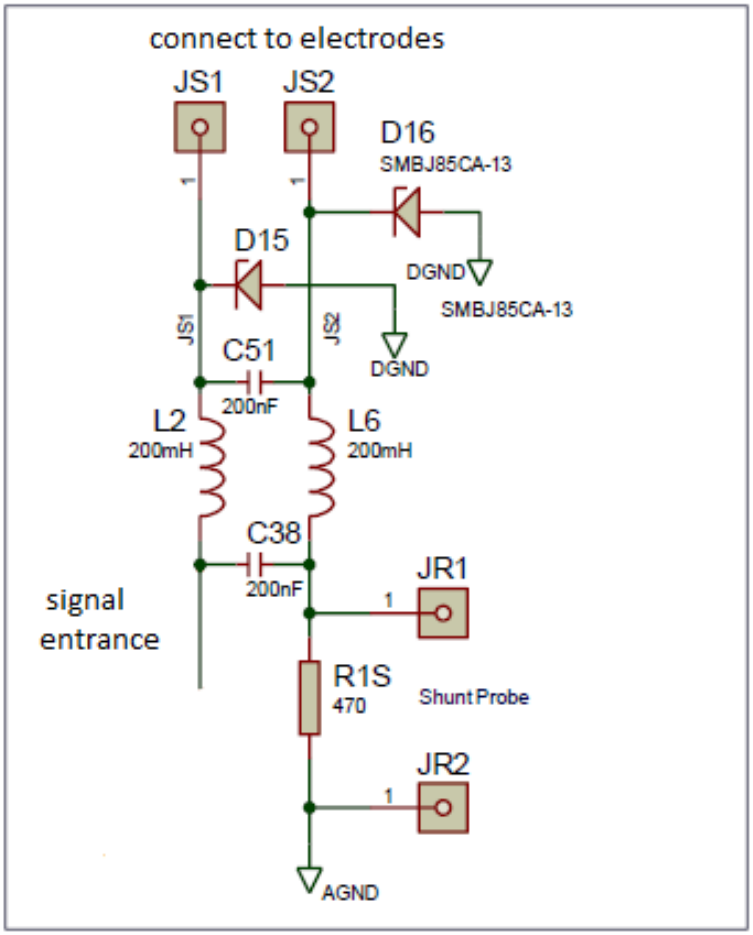

Figure 10: Excerpt from the stimulation circuit, showing the connecting electrodes, which apply the electrical current on the patient.

Source: Own authorship.

The circuitry shown in figure 10 is part of the PCB which is placed in the MRI room within the rack to further shield the circuit from electromagnetic and radio frequency interference. The low pass LC-filter shown above protects the circuit from the MRI RF-pulses which could enter the circuitry through the wires connecting to the two electrodes. The cut-off frequency ranges around 40-50Hz to shield both the mains voltage and the RF pulses.

The electrode, wire and filter design has already been investigated and determined in previous research projects conducted by Manczak and Della Justina (for more detailed information see (MANCZAK, 2012) and (JUSTINA, 2014)). Circular electrodes with an area of approximately $9cm^2$ fixed through adhesive tape showed to be the most appropriate electrodes for GVS research. They are connected to 30 cm carbon wires to prevent interference of the wire with the magnetic imaging of the head. Carbon is not ferromagnetic and does thus not generate

artifacts in the MR images. Conducting wires connect the carbon wires to the stimulator. As the conducting wires pick up RF pulses and thus induce a current a topology of low pass LC filters is placed along the conducting wires to prevent this induction of current and noise.

3.3 CONTROL CIRCUIT DESIGN

After having outlined the design and implementation of the stimulation circuit, the next step is the depiction of the control circuit. The control unit can be divided into four parts: the microcontroller explained in subsection 3.3.1, the optical communication between PC and microcontroller, further depicted in subsection 3.3.2, the design of the communication protocol, shown in subsection 3.3.3, and finally the development and implementation of the associated firmware, presented in subsection 3.3.4.

The control circuit is entwined with the stimulation and security circuits. Still, a division can be made according to the tasks of the different circuits. The further described control circuit depicts all functionalities related to the supervision of especially the stimulation but also to the security.

3.3.1 MSP

Before going into detail about the description of the control circuit design, this short subsection aims to point out the main characteristics of the MSP used within this thesis. As there is a great number of possibilities when it comes to microcontrollers, there are always some personal decisions besides the thesis specific requirements. The first choice was to use a microcontroller of Texas Instruments' mixed signal microcontroller family. This choice was made because of existing knowledge and experience with it. Besides that, Texas Instruments provides a huge and convenient driver lib, allowing C-Programming on their microcontrollers of this family. Various programming examples help during the process of firmware development. After this first decision, the required features enclose an even fewer number of possible devices out of which a convenient one is picked. The features which are important for the realization of this thesis are as follow:

- Low supply voltage.
- Ultra-Low-Power.
- Universal Serial Communication Interface.

- Analog-Digital-Converter.
- Digital-Analog-Converter.
- Internal DMA.
- Internal Timer.

All these requirements are met with the MSP430F5359 (TEXAS INSTRUMENTS INCORPORATED, 2013). The functional block diagram of the MSP430F5359 is shown in figure 11.

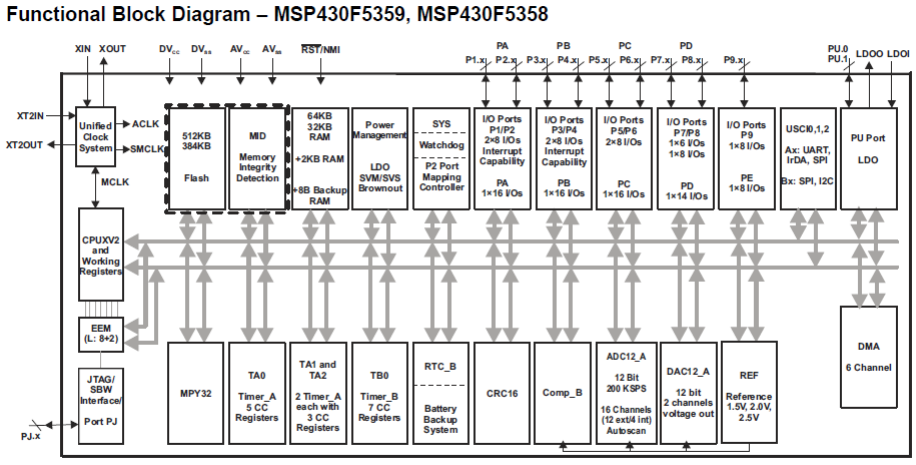

Figure 11: Figure of the block diagram of the microcontroller MSP430F5359.
Source: MSP430F5359 datasheet, Texas Instruments Incorporated

3.3.2 OPTICAL COMMUNICATION

The GVS is used during the fMRI study. One key requirement is the development of a project design that generates a minimum interference with the magnetic imaging and is maximally shielded against electromagnetic interference (EMI) and radio frequency interference (RFI).

To face these requirements, the communication channel within this project is implemented as optical communication using fiber optic cables. This avoids the use of wires that lead from the control room into the fMRI room and which could pick up signals from the MRI RF-pulses. The project design uses two fiber optic cables, one for each communication direction. The communication design is fully one-directional so that two fiber optic cables need

to be used to allow messaging and responding. No halfduplex or fullduplex characteristics of the fiber optic cables is currently being used in this thesis. Each side of the fiber optic cable provides one optical receiver and one optical transmitter. This project employs receiver and transmitter fabricated by Avago Technologies (AVAGO TECHNOLOGIES, 2011). The HFBR0500Z series convinced because of the easy circuit integration and the purpose of solving problems with EMI/RFI immunity. The following figure 12 and figure 13 show the functions of the pin connections of optical transmitter and receiver.

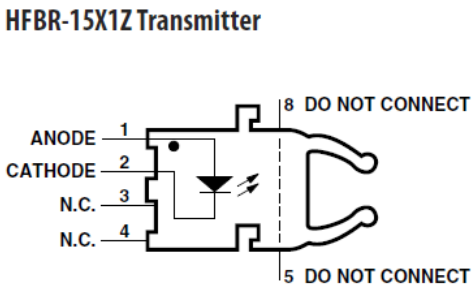

Figure 12: Figure of the optical transmitter HFBR1521Z.

Source: HFBR0500Z data sheet, Avago Technologies

The optical transmitter converts the voltage difference applied between anode and cathode into an optical signal by driving a LED with 660 nm wavelength that enters the fiber optic cable. The driving circuit is shown in figure 14.

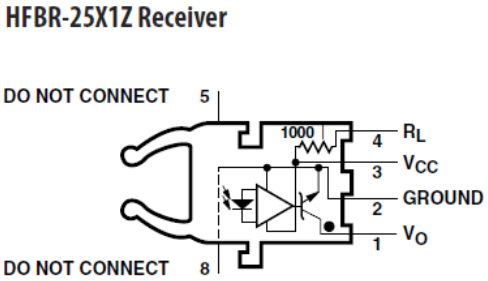

Figure 13: Figure of the optical receiver HFBR2521Z.

Source: HFBR0500Z data sheet, Avago Technologies

On the receiver side, the photo diode converts the received light transmitted via a fiber optic cable into an according current. This current drives the bipolar junction transistor included in the HFBR2521Z and generates a voltage difference between V_{out} (output voltage pin) and Ground. Pin 1 and 4 provide the data output pins as can be seen in figure 13.

The technical data sheet provided by Avago Technologies supplies exemplary driving circuitry which have been modified for the utilization in the galvanic vestibular stimulator.

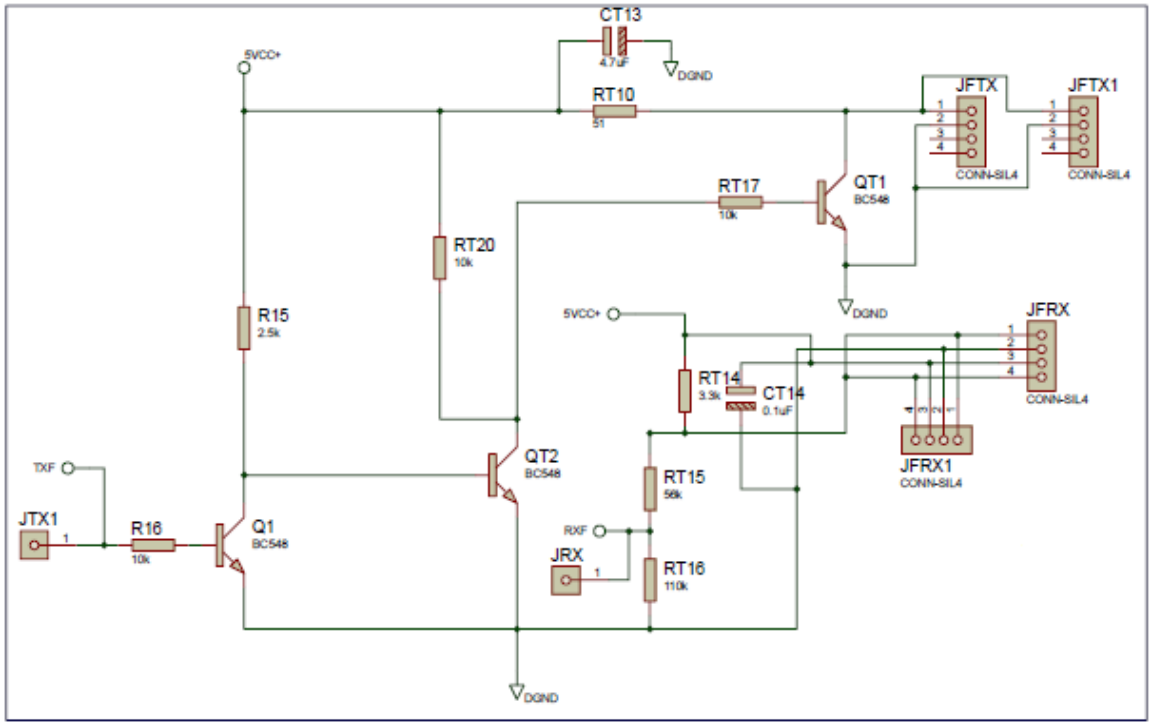

Figure 14: Part of a circuit schematic of the current source depicting the optical transmission and reception circuitry. The transmitter signal is generated by one of the MSP output ports and is applied to jumper JTX1. This signal is then turned on and off the current that drives the LED. The receiver LED is sampled through the RT15 and RT16 resistance divider at jumper JRX.

Source: Own authorship

The transmission data which is the communication protocol data in this project is generated by the microcontroller of the current source circuit. Resistor RT10 of 51 Ω is used to limit the electrical current through the LED connected to pins 1 and 2 of the optical transmitter. QT1 bypasses the LED current, depending on the signal that is applied at JTX1 and drives Q1 and QT2. The desired information is now transmitted as an optical signal via fiber optic cable and can be received on the other side of the cable by the optical receiver.

The optical receiver provides the data on pin 1 and 4. As the voltage output ranges between 0 V and 5 V (which equals the positive voltage supply), a resistor divisor, RT15 and RT16, is needed to connect this signal to the MSP analogue-to-digital converter (ADC) which has a range from 0 V to 3.3 V.

3.3.3 PROTOCOL DESIGN

As already explained before, the connection and interaction between PC and MSP is established via optical communication. This functionality shall be given without continuous interaction with the user. To guarantee the proper function and the working communication, a communication protocol was developed.

The communication sequence is determined through the definition of a fixed protocol structure and different operation codes for both commands and acknowledgment answers. This subsection presents the protocol structure and the communication characteristics determined for this thesis. A detailed specification of the communication protocol can be found in the appendix.

At first, the communication canal has been determined to be serial. The communication interface is optical as has been outlined in subsection 3.3.2. The main characteristics for serial communication, i.e. the baud rate, the parity and the number of stop bits, were determined to be 9600 baud, without parity and one stop bit. A parity bit would be an option to check the transmitted data for errors. This protocol structure provides the data check in the form of a determined data field for the cyclic redundancy check byte (CRC). The communication protocol specification is divided into two groups. One group contains all possible data structures sent from the PC to the MSP while the other group provides the operation codes for the opposite communication direction.

The communication within this thesis is designed to follow a master-slave topology where the PC constitutes the master and the MSP represents the slave. This way all control lies on the PC and user side. Hence, the communication data sent by the MSP are solely responses to the protocols received by them before. The two groups of data structure mainly differ in the operation code.

In most cases the communication protocol consists of five bytes, as shown in figure 15.

SFD	SFD	Opcode	Length	CRC

Figure 15: Normal protocol structure

Source: Own authorship

The first two bytes of the protocol are called SFD (which stands for *start frame delimiter* and origins in the Ethernet frame definition) and contain fixed values for every protocol frame in this project. In sequence, the operation code (abbreviated as opcode) is given.

Every command from PC to MSP is represented as a specified operation code. All messages sent from MSP to PC are responses to the commands received so that the operation codes go with the according command. This way, the connection between command and answer is represented.

The different operation codes are explained in the detailed specification given in the appendix. A list of the different operation codes for messages between PC and MSP and vice versa is shown in figures 16 and 17.

Opcode	**Description**
00h	Ping
01h	Stimulation Setup
02h	Start Stimulation
03h	Halt Stimulation
04h	Sleep
05h	Wakeup
06h	Stimulation Data Request

Figure 16: List of operation codes for commands sent by the PC.

Source: Own authorship

The list of operation codes sent by the PC forms a sequence beginning with number 00h and ending with 06h. The *Ping* command only checks the communication with the MSP. The *stimulation setup* command (01h) sends the next stimulation configuration to the MSP and thus must contain the data field. 02h and 03h represent the commands to start and respectively halt the stimulation. The *sleep* and *wakeup* commands (04h and 05h) disable or activate the MSP itself which might enter a low power mode when it is not being used. The last possible command (06h) is the request for stimulation data, e.g. the feedback data obtained by the MSP.

The following figure 17 presents the counterpart to the operation codes of the PC on the MSP side.

In the same sequence as the list of commands, the MSP uses operation codes to respond to the tasks received. The message containing a data field here corresponds to an opcode of 26h, which represents the response to the stimulation data request. The data field contains all feedback data. The detailed description of the data field can be found in subsection 3.3.4 and section 3.5.

The fourth byte determines the length of the optional data field. Within most protocol structures implemented in this thesis this fourth byte equals zero. Figure 18 presents a protocol

Opcode	Description
20h	Answer to Ping
21h	Stimulation Ready
22h	Stimulation Started
23h	Stimulation Halted
24h	Sleeping
25h	Awaken
26h	Stimulation Data

Figure 17: List of operation codes for answers sent by the MSP.

Source: Own authorship

structure containing the data field beginning at byte five.

SFD	SFD	Opcode	Length	Data	CRC

Figure 18: Protocol structure with data field

Source: Own authorship

The last byte of every protocol structure is the CRC byte as already stated in a previous paragraph. The CRC differs for every operation code and data byte because it is calculated in accordance with the bytes contained in the current protocol. The CRC is calculated through a bit by bit XOR operation on all previous protocol fields except for the two SFD bytes. For all protocol structures that do not include a data field, the CRC equals the operation code because the XOR operation will result in a high level if the two bits being compared differ from one another and will result in a low level if the two bits are equal. In case there is no data field included in the protocol, the length is zero so that the XOR operation is just applied to 0x00 (the length) and the operation code. The CRC is thus a way to check the correct transmission of the operation code. If a data field is included, the CRC will take the data field into account as well and will give the check sum of all varying bytes sent.

3.3.4 FIRMWARE

The firmware constitutes the intelligence of the control circuit. It can be seen as the counterpart to the software which allows the interaction with the user. Still, the firmware itself does not enable any dynamic interaction. It offers the control of the current source according to the settings made by the user and enables the various measurements such as battery level monitoring or feedback measurement.

The different firmware states depicted in the previous subsection 3.3.3 are implemented in the firmware and entered through function calls following the data reception. The main functions of the firmware are presented in figure 19. For a better overview, the return values and parameters are not shown here. The graphic solely shows the function sequence for the communication handling and data acquisition. The diagram represents each main function as one block. Thus not every function implemented in the firmware is depicted here.

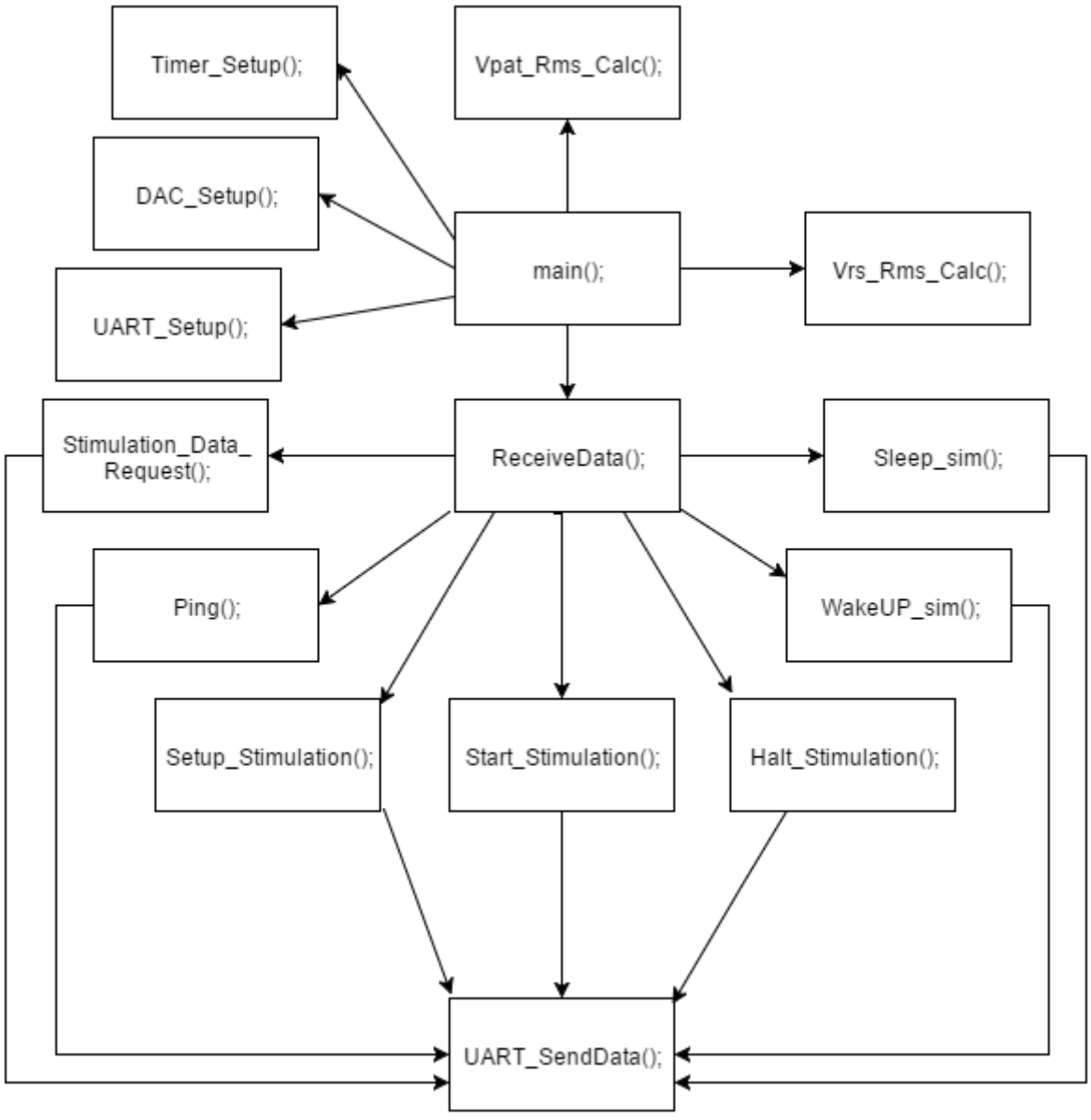

Figure 19: Block diagram of the main functions of the firmware. Possible function sequences are presented ignoring return values and parameters.

Source: Own authorship

After having outlined the communication structure and protocol, the according firmware structure is presented here. Due to the master-slave topology for communication,

the main functionalities of the firmware are initiated by the according command sent by the PC. Thus, the function to receive data from the PC is the center of the firmware. Having checked and processed the received data the next function is called to establish the subsequent firmware state and perform the instructed action such as configuring the DAC for the stimulation setup or sending the MSP to enter a low power mode (”Sleep”). According to the communication protocol definition, the firmware has to send an acknowledging answer to the PC. The sequence hence terminates with the function to send data via UART, the universal asynchronous receiver transmitter.

Two other main functionalities are represented through the calculation of the root mean square (rms) value of the electric voltage at the shunt resistor and at the patient. The calculated values are needed for accurate patient monitoring and feedback measurement which are returned as answers to the *stimulation data request* command.

An activity diagram describing the structured process of the firmware can be found in the appendix. It is more extensive than the previous block diagram and offers a brief but significant overview of the firmware structure.

After powering on, the firmware enables the hardware. The enabling is done through I/O pins connecting to enable pins of various ICs. DAC, ADC and UART are configured and the according MSP pins are set as output and respectively input pins. If necessary, interrupts are being enabled which are especially important for the use of the UART and the DMA. The firmware mainly awaits the occurrence of an event. This can be either from one of the DMA channels or from the UART data reception buffer. If the event is caused by one of the DMA channels, the converted value will be used to calculate the desired value linked to the measured one. For instance, the converted value given by DMA channel 1 is used to calculate the rms voltage across the patient. A UART interruption arises after the reception of new data from the PC. The message is then processed, extracting the operation code in order to initiate the adequate function call and peripheral action. The firmware holds a list of possible operation codes. If the received operation code is none of the operations codes in the list, the message will be discarded. According to the operation codes of the received messages different actions are initiated and different functions called. Terminating the first actions, the firmware creates the response and then sends it to the PC. After that, the firmware returns to the state of awaiting an event.

There are two possibilities terminating the firmware which result in the entering of a sleep mode. This is a lower power mode which only leaves some peripherals enabled for the wake up signals. The first way to terminate the firmware is a communication timeout. If no

new message is received from the PC in more than five seconds, a loss of the communication connection will be assumed. During stimulation, the firmware would conduct the current stimulation setup until it times out as well and then it would terminate the stimulation and disable the hardware circuitry. Another possible ending point is the reception of the *sleep* command. The converters are halted and the DMA is disabled. All circuitry is then disabled after having sent the response to the PC.

3.3.5 PGA CONFIGURATION

This section describes the hardware and the firmware development to control the gain of the two PGAs used to measure the voltage across the shunt resistor and the voltage applied to the subject by the current source. The maximum voltage range is determined through the maximum input voltage at the DAC of the MSP which is 3 V. To provide a maximum ADC precision, the gain of the PGAs must be adjusted according to the applied current so that the measured voltage is not too small and does not exceed the maximum voltage range of the ADC.

Figure 20 presents the circuit conditioning the electrical current source. The input signal is provided by the DAC of the MSP. In order to remove the 1.5 V DC level, a subtracter, implemented through operational amplifier U16B, is included into the circuit. The subtracter has a gain of 3.65.

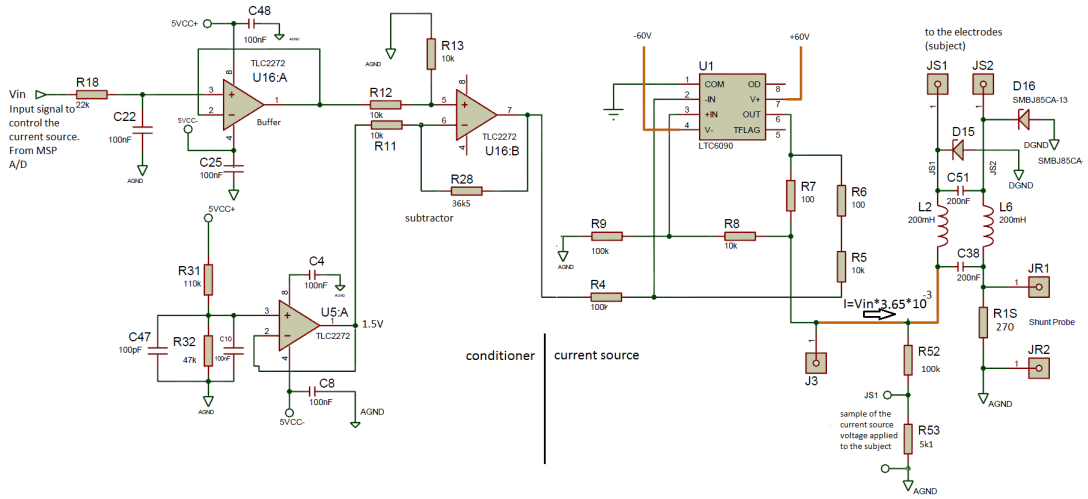

Figure 20: Extract from the current source circuit showing the electrical circuit that conditions the stimulation signal provided by the MSP ADC. The subtracter included in the circuit removes the 1.5 V DC level. Then the signal is applied to the current source input pins. The amplified current source output voltage is then applied to the subject.

Source: Own authorship

The following equation presents the calculation of the voltage across the shunt resistor

as a function of the signal amplitude V_{in} provided by the DAC of the MSP and the conditioning circuit.

$$V_{Rs} = V_{in} * 3.65 * 10^{-3} * 270$$

Where 3.65 is the operational amplifier gain (figure 21, U16A), 10^{-3} is the current conversion factor (see 3.2.1) and 270 is the shunt resistor value. It can be simplified by the following equation:

$$V_{Rs} = 0.99 * V_{in}$$

Figure 21 shows the electronic circuit to measure the voltage across the shunt resistor. It is buffered and applied to the PGAs. An adder circuit (figure 21, U14:A) adds a DC level of 1.5 V to the measured voltage. The output of the adder is applied to the ADC of the MSP. Based on these equations, the PGA gain values are previously determined according to the desired current amplitudes. Table 2 contains the data obtained in laboratory tests. The first column contains the desired current amplitudes, with a range from 0.5 mA to 5.0 mA. The second column presents the theoretical peak voltage values which are directly proportional to the applied current amplitude. Column three contains the measured voltage across the shunt resistor already amplified by the PGA. In column four, the correspondent PGA gain value is defined. The last column shows the practical values for the patient voltage that are closest to the desired values previously shown in column two.

Desired current A_p	Theoretical V_p for A_p (AC)	measured V_{Rs} with gain	V_{Rs} PGA gain	Practical V_P for A_P (AC)
0.5 mA	0.14 V	2.46 V	7	-
1 mA	0.27 V	2.87 V	5	-
1.5 mA	0.41 V	2.74 V	3	0.48
2 mA	0.55 V	2.60 V	2	0.65
2.5 mA	0.68 V	2.87 V	2	0.8
3 mA	0.82 V	2.32 V	1	1
3.5 mA	0.96 V	2.46 V	1	1.2
4 mA	1.10 V	2.60 V	1	1.4
4.5 mA	1.23 V	2.73 V	1	-
5 mA	1.37 V	2.87 V	1	-

Table 2: Correlation between the desired current, the theoretical and practical PGA gain for a V_P resulting in the correct A_P

Source: Own authorship

The current source applies a relative high voltage to the patient since its impedance is approximately 10 kΩ. Thus, it is necessary to include a resistor divider to sample the applied voltage and apply it to the ADC of the MSP. Also, since the impedance differs among different

subjects and electrical currents, the PGA gain must be adjusted to use the maximum possible ADC conversion range. In figure 20, the resistor divider between R52 and R53 provides the sample of the output voltage applied to the subject by the current source.

Table 3 below shows the correlation between the voltage applied to the patient and the PGA gain. The first column presents the different values for V_P, the measured peak voltage across R53. The second column contains the gain of the PGA that results in the maximum voltage value possible which is shown in column three.

when $V_P <$	gain	max. possible value
1.71 V	7	2.97 V
1.75 V	6	3 V
1.8 V	5	3 V
1.875 V	4	3 V
2 V	3	3 V
2.25 V	2	3 V
2.25 V	1	V_{P-}

Table 3: Correlation of the voltage across the patient and the correspondent PGA gain values to reach the highest possible precision.

Source: Own authorship

Figure 21 shows an extract from the stimulation circuit showing the feedback measurement across the shunt resistor. The PGA enables the gain adjustment to amplify the measured current so that it optimally exploits the voltage range at the MSP ADC input. Three MSP output pins are connected to a driver which converts the 3.3 V High level into a 5 V High level. Therefore, the MSP output pins can set the PGA gain pins adjusting the gain to the desired value. The implementation of the PGA is shown in figure 21.

The configuration of the PGA gain for the amplification of the voltage across the shunt resistor is done in the *start stimulation* function of the firmware. Through the configuration of the current setup, the amplitude of the current to be applied is known. That way, the appropriate gain can already be set before the actual measurement to guarantee that the measured voltage across the shunt resistor can be determined with the highest precision possible.

The controlling of the gain for the measurement of the voltage across the patient is done dynamically. After the *start stimulation* command the gain is set to 1. In the first DMA interrupt the function *VpatrmsCalculation* is called. The function verifies the peak value of the voltage across the patient. Depending on the value, the gain is adjusted or not.

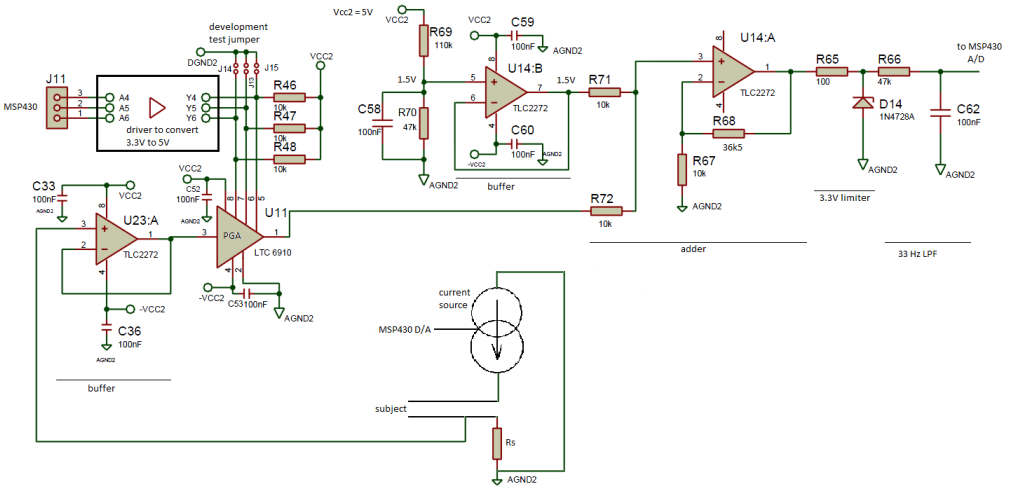

Figure 21: Extract from the feedback measurement circuit, containing the PGA to adjust the amplification of the measured voltage across the shunt resistor. Three MSP output pins drive the PGA gain configuration pins.

Source: Own authorship

3.4 PROTECTION CIRCUIT DESIGN

Another important part of this thesis is the design and development of a protection circuit. In medical equipment it is crucial to ensure the health and safety of both patient and medical staff. Even for this application in medical research with a prototype, maximal health and safety measures must be ensured during the whole handling and function of the device. Despite the software and firmware securing the correct state of the current source and battery level, a second circuit was designed to add a second layer of analogue and digital protection. This section provides an overview of the different parts of the protection circuit: the measurement and auto regulation of the stimulation characteristics in subsection 3.4.1, the overcurrent protection in subsection 3.4.2, the design and inclusion of a patient button for patient monitoring in subsection 3.4.3 and a monitoring of the current battery level in subsection 3.4.4. The design and implementation of the protection circuit is depicted in extracts from the circuit schematic and its explanation.

3.4.1 FEEDBACK AND REGULATION

One main amendment of this master thesis in comparison to the preceding master thesis of Tiago Manczak (2012) was the inclusion of a feedback measurement and an auto regulation

intelligence that were implemented to protect the subject against any overcurrent. The main part of the auto regulation intelligence has already been shown in subsection 3.3.4. As a further characteristic the hardware enables a variable configuration and regulation, which is presented here.

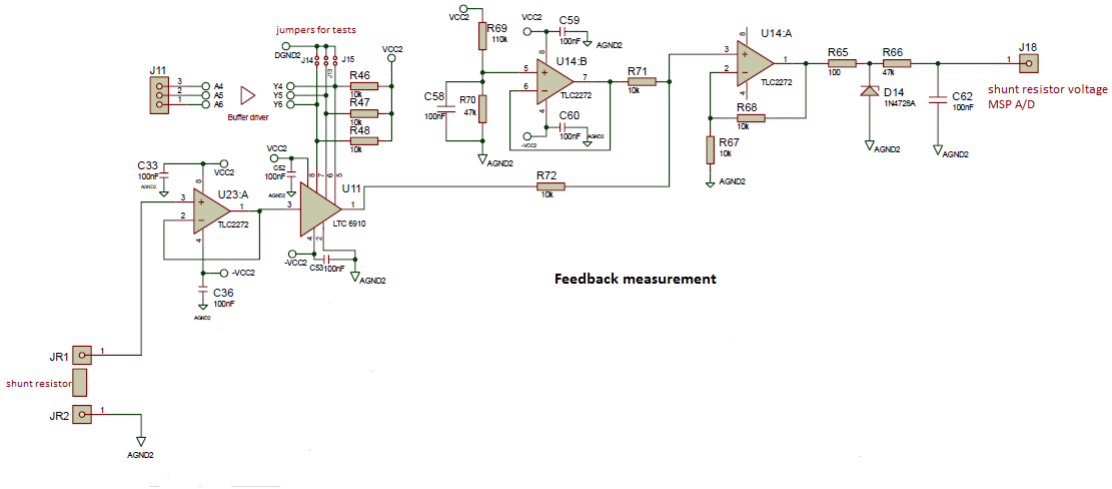

Figure 22: Extract from the protection circuit: measurement of the current applied to the patient.

Source: Own authorship

Figure 22 shows an extract from the protection circuit which provides information about the electrical current measurement. The current applied to the patient is measured as a voltage across the shunt resistor R_s, see figure 21, connected in sequence to the patient. The measured voltage (the feedback) passes a digital programmable gain amplifier (PGA) and is magnified. The PGA used here is the LTC6910-3 provided by Linear Technology (LINEAR TECHNOLOGIES, 2002). Its gain ranges between 0 $\frac{V}{V}$ and 7 $\frac{V}{V}$ as is shown in the datasheet. The gain depends on the setting of pins 5, 6 and 7 that are connected to the MSP via an IC translating the input voltage of 3.3 V provided by the MSP ports to a 5 V output voltage driving the PGA pins. The used IC is a buffer/driver with open-drain outputs provided by Texas Instruments Incorporated, designated as SN74LVC07A (TEXAS INSTRUMENTS INCORPORATED, 2015). The amplification applied by the PGA was tested in the laboratory. The pins configuring the PGA are set by the MSP so that the firmware directly controls the PGA. The voltage across R_s is then clamped to a 1.5 V DC level (see U14:A and U14:B in figure 22) and enters the canal of the ADC of the MSP for conversion. The resistance value is known to be 270 Ω so that the firmware is then able to calculate the amplitude of the current. Any further adjustment for auto regulation is done by the firmware.

3.4.2 OVERCURRENT PROTECTION

Research showed that there is a maximum current which can be applied to the patient without causing too much pain or a strong feeling of discomfort. The current amplitude in this project shall be limited to 5 mA according to the previous tests and research results (MANCZAK, 2012).

Besides the current monitoring done by the MSP, we also implemented a hardware electrical current limitation for safety reasons. The hardware current limitation is implemented through a bistable relay provided by Tyco Electronics Corporation with the designator V23079 (TYCO ELECTRONICS CORPORATION, 2015). If the applied current exceeds the limit, the state of the relay will change and will short-circuit the current source. Thus, the current is no longer applied to the subject. The relay can only be reset through the MSP, by applying a high level on one pin.

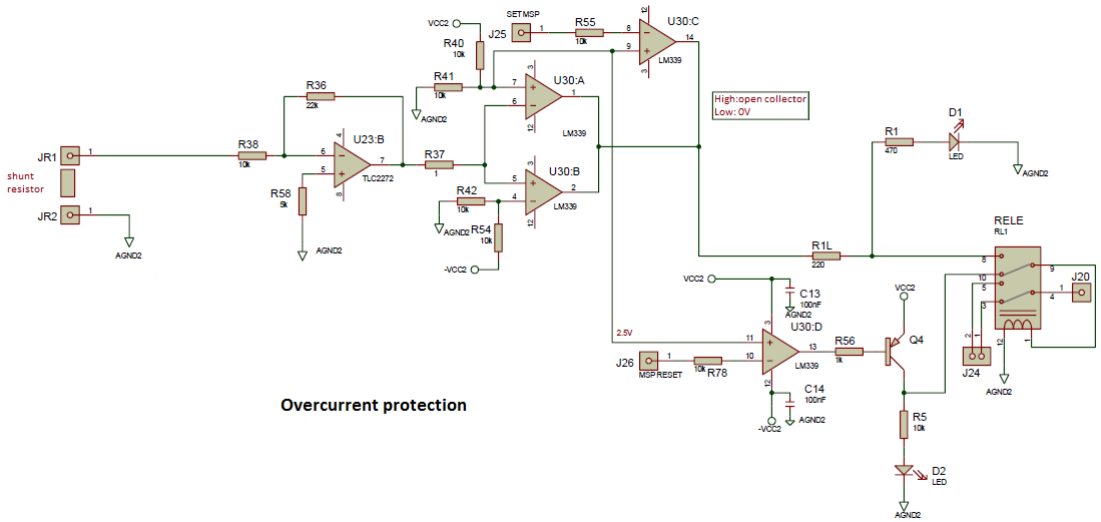

Figure 23: Extract of the protection circuit: overcurrent detection and patient protection via relay.

Source: Own authorship

Figure 23 shows the overcurrent detection and the inclusion of the relay in the protection circuit. The overcurrent detection is located on the shunt resistor. To determine the applied current, the voltage on the resistor is measured and then amplified. The relay can be set either by a high level on an output pin of the MSP or by a high level at the output of a Schmitt trigger comparator comparator (as shown in U30:a and U30:B in figure 23). The comparators used in this project are quad differential comparators provided by Texas Instruments under the LM339 specification. Setting the relay causes a switch within the relay to toggle. The current

source output is then short-circuited and the stimulation is interrupted.

As the voltage across the patient then drops to zero, the user is alerted on the PC screen that an overcurrent occurred. The relay can only be reset by the firmware through a command sent by the user through the user interface. This happens automatically as part of the auto regulation. The protection design relinquishes any user interaction to accelerate the process of reset.

The firmware controls the protection relay as outlined before. Therefore, a defined state of the relay during circuit initialization must be guaranteed. This can be done by the firmware driving J25 and J26 (shown in figure 23) to low level and then driving J26 to high level. The relay then short circuits the patient and guarantees his safety. On the other hand, the state of the relay is determined, being in state *Reset*. If the relay already was in state *Set* before, it would now be in state *Set*. If it already was in state *Reset*, it would remain in this state. To enable the stimulation, J26 is driven to low level and J25 is driven high during three seconds. This way, the relay is transferred to state *Set* and the patient is included in the circuit. After the end of the stimulation or in case of an emergency, the relay is again transferred into the state *Reset* for security reasons.

3.4.3 PATIENT BUTTON

Another protection unit in the shape of a patient button was included in the project. The patient button was built with a normally closed switch placed in parallel with the subject. Thus, when pressing the button, it lets the electrical current flow to the subject, otherwise it prevents the electrical current from flowing through the subject. In case of any discomfort during the stimulation sequence, the patient releases the patient button. It is designed in such a way that when the subject removes its hand and the button is released, the output of the current source is short-circuited. In the event that the patient passes out or experiences intense pain or discomfort, he would immediately stop pressing the button. By releasing the button, a short circuit stops the electrical stimulation of the subject. This way the patient has full control over the examination and could interrupt the stimulation at any given time. It is important that the patient button is realized in a passive way so that the protection can be guaranteed without any action or force.

Similar to the feedback measurement, the voltage applied to the patient by the electrical current source is measured in order to determine the patient button state. As a released button short-circuits the stimulation circuit and thus no current is applied to the patient, the voltage applied by the electrical current source is approximately zero. The voltage applied by the

electrical current source is relatively high and cannot be applied to the ADC input of the MSP, thus a voltage divider, implemented through R52 and R53, shown in 24, is used to reduce this voltage. The patient button is placed along the wire that connects the subject and the electrical current source. Therefore, when the button is released, the resistor R_p is short-circuited and the voltage measured by the ADC of the MSP is the voltage across the resistor R_s, that is placed in series with the subject and that is used to monitor the stimulating current.

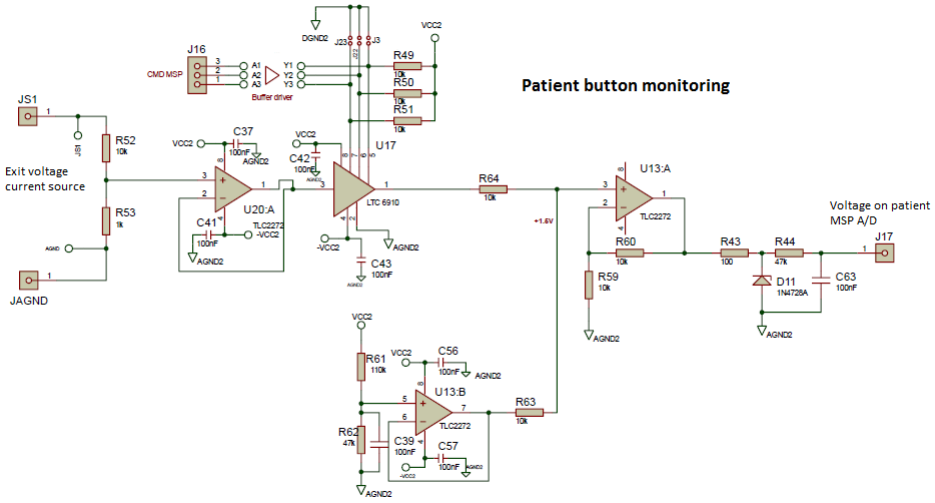

Figure 24: Extract from the protection circuit: measurement of the patient button state.
Source: Own authorship

Figure 24 presents an extract from the protection circuit schematic showing the hardware implementation of the patient button monitoring. It shows that the circuit is basically the same as the one for the feedback measurement. Only the point of measurement is different as the patient button monitoring directly supervises the voltage on the patient himself, while the feedback circuit measures the voltage on the shunt resistor.

The measured voltage is amplified by a PGA and then again by an operational amplifier until reaching an ADC canal of the MSP. The firmware interprets the converted signal and alerts the user on the PC screen about a released patient button.

3.4.4 BATTERY MONITORING

The whole circuit runs on a 9 V battery, supplying the current source circuit and another 9 V battery, providing the supply voltage for the security circuit. These two circuits are independent and isolated from one another. The independence of the two circuits is crucial to provide all security functions especially in case of errors on the other circuitry.

Figure 25 shows the voltage supply by the 9 V battery. Pins V12 and V12b constitute the pins for the flyback voltage supply and the voltage supply for the rest of the circuit.

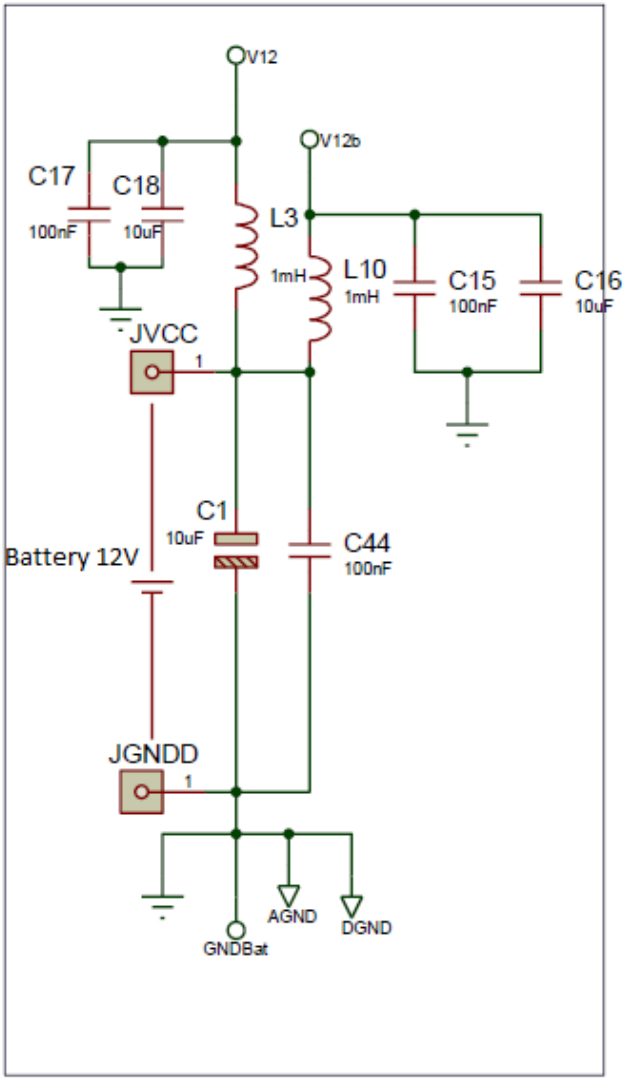

Figure 25: Battery circuit with 9 V battery

Source: Own authorship

In order to provide the required supply voltages, it is crucial to guarantee a sufficient battery level. Monitoring the battery level during the stimulation process provides continuous information about the battery status. The user might monitor the battery via the graphical user interface (GUI) and sees the current battery level on the PC screen. At its maximum the battery level is approximately 9 V. To convert it via ADC, the voltage must be smaller than a maximum voltage of 3.3 V. A voltage divider followed by a voltage follower picks up the voltage in the right range and passes it on to the ADC of the MSP.

The battery monitoring for the protection circuit is designed equally. The only

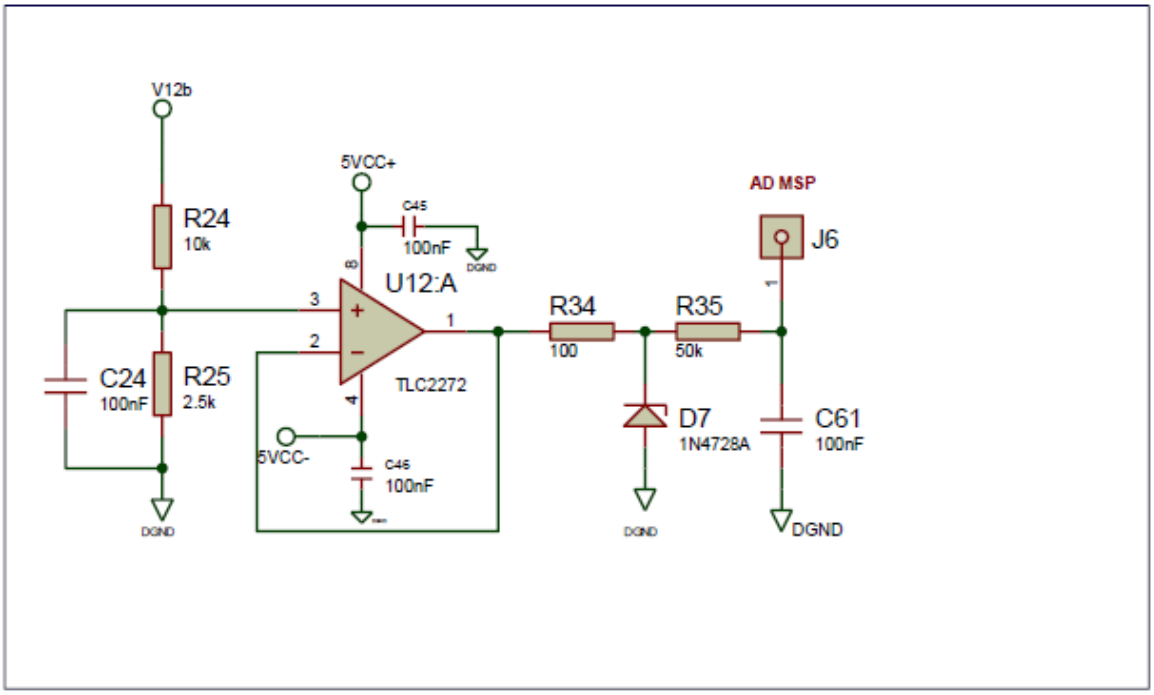

Figure 26: Circuit for measurement of the battery voltage

Source: Own authorship

difference is the battery level, which should be approximately 9 V. This second circuitry is not shown here for reasons of repetition.

3.5 SOFTWARE

Having outlined the implementation and design of hardware and firmware, this chapter focuses on the software concept and its implementation. The software faces three main requirements: Creation of an easy and comprehensible graphical user interface for the interaction with the user, implementation of a communication interface for communication with the firmware and enabling of the functionality of both software and the whole device.

Subsections 3.5.1, 3.5.2 and 3.5.3 present a detailed description of the design and implementation process.

3.5.1 GRAPHICAL USER INTERFACE

The GUI represents the interface between the user and the software itself. It masks the underlying program and facilitates the user interaction and program handling for the user. During GVS, the supervising physician controls and conducts the examination. As already

explained in the previous subsections 3.3.3 and 3.3.4, the firmware only reacts on commands sent by the software. Thus, the control merges in the GUI. The GUI for the GVS therefore has to include three main functionalities:

- Connection configuration,
- Stimulus configuration and
- Trigger control.

The GUI programming is realized with the help of the Qt plug-in for Microsoft Visual Studio Professional 2013. In Visual Studio, the software version 12.0.40629.00 Update 5 is being used. Qt Add-in 1.2.4 of Qt version 5.5.0 is included in the Microsoft Visual Studio Professional 2013. The Qt cross-platform application framework is being used for application programming, permitting the user to generate applications in the style of the different underlying operating systems. It is currently open for use under open-source license. The Qt Add-in provides an easy-to-use user interface to design the desired application GUI.

The first step when starting the application for stimulation examination is to establish a communication connection between PC and MSP board. The communication between these two parts is established via serial communication through optical fibers. Thereby the software is connected to a COM port via a USB port. The user only determines the COM port that connects to the hardware board containing the optical transmitter and receiver. He is able to start and respectively stop the COM port connection. The serial communication needs a determination of baud rate and message configurations (such as number of data bits, number of stop bits and parity) which are specified in the communication protocol that is already implemented within the code. The connection configuration interface seen by the user looks as shown in figure 27:

A very important feature is the screen that logs the communication establishment. The user can verify whether the connection to the COM port has been established without problems or whether it receives error messages during the process of an ongoing stimulation sequence. This augments the program's visibility for the user and helps detecting flaws during the stimulation. The log can be saved for later interpretation.

After having established a connection between PC and optical transmitter and receiver board, the communication connection is already open for all possible commands. The user now configures the desired stimulation characteristics and sequence. The GUI for stimulation configuration already includes galvanic stimulation limits and the determined resolution for the stimulation current variation. The adjustable values are:

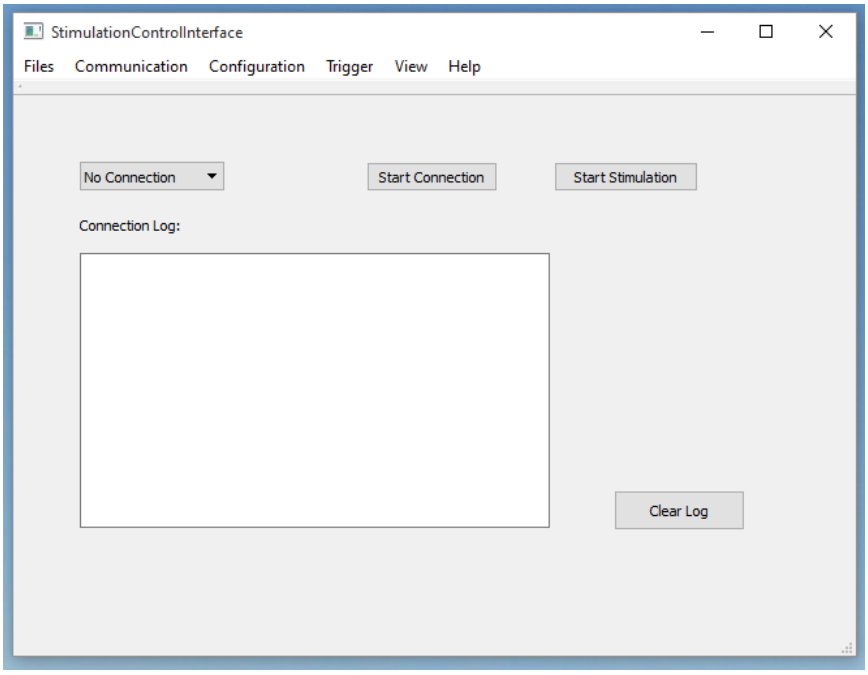

Figure 27: Graphical User Interface: Connection Widget

Source: Own authorship

- Number of repetitions of the whole stimulation sequence,
- Number of repetitions of one stimulus configuration,
- Stimulus wave form,
- Stimulus amplitude,
- Stimulus frequency,
- Time in minutes of the configured stimulus,
- Time in seconds of the configured stimulus.

Moreover, the user decides which stimulation configurations are part of the stimulation sequence. After finishing the configuration, checking the 'configuration done' box terminates the configuration and disables all further adjustments. Another option for the stimulation configuration is to load a previously saved stimulation sequence into the current setting and use or modify the stimulation characteristics. Every configuration made can be saved as a new stimulation group or replace an already existing one. The stimulation configuration GUI is shown in figure 28 as shown below.

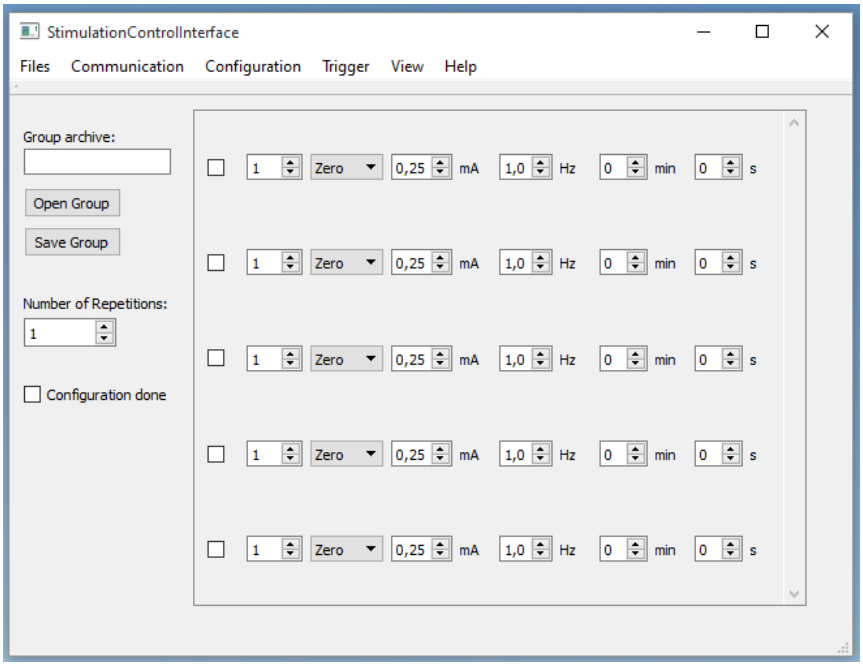

Figure 28: Graphical User Interface: Configuration Widget

Source: Own authorship

For the program to be able to start, the user has to determine the possible and desired input trigger. The software provides two possible trigger inputs: A trigger signal received by the MRI signal or a manually generated trigger which must be guaranteed by the user himself. The trigger is being selected in the following trigger configuration widget, presented in figure 29.

In case of a manual trigger, the user controls both devices, the MRI and the GVS. Therefore, the user has to define a delay in seconds to be included before sending the starting command to the MSP. This is because the MRI includes a delay between the reception of the *start* command and the first acquired volume. To guarantee a synchronization of the MRI data acquisition and the stimulation control done by the MSP, the adjustment of the adequate delay time is crucial.

Additionally, the GUI widgets, already shown in the interface, contain features to represent the measured feedback values in a pop-up window. That way, the user is able to monitor the feedback while observing the communication log. The shown values are the number of pending volumes to be acquired, the stimulation values, such as current amplitude, current frequency, the tapped voltage on the load resistance and the electrode impedance. Moreover, the window shows the level of the battery to prevent the risk of a low battery. The feedback window is shown in figure 30. The underlying program intelligence is featured in the subsection 3.5.3.

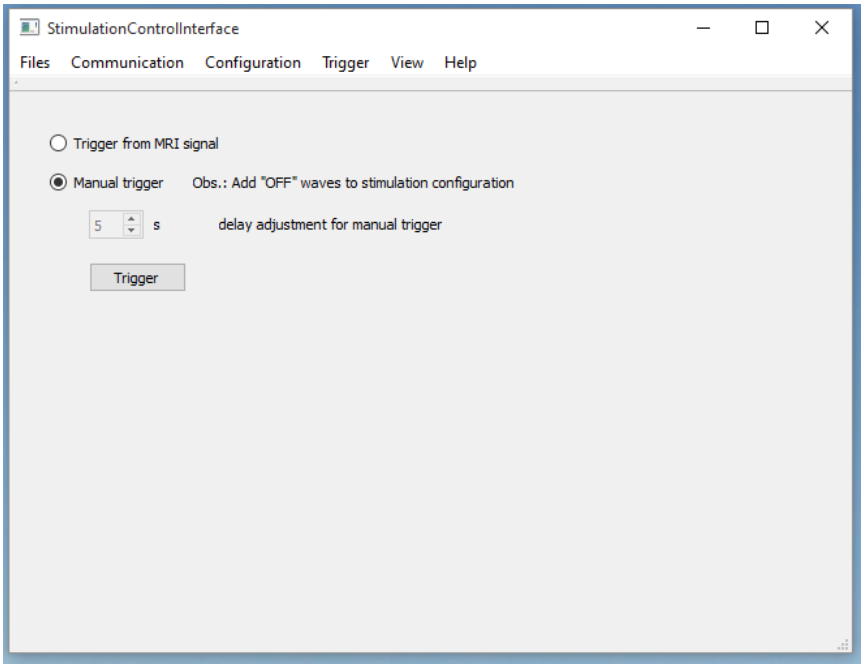

Figure 29: Graphical User Interface: Trigger Widget

Source: Own authorship

3.5.2 COMMUNICATION

The implementation of the communication between MSP and PC has already been featured in 3.3.3 and 3.3.4. After outlining the protocol design in 3.3.3 and presenting the firmware implementation of the communication protocol, this subsection depicts the implementation of the communication protocol in the software.

Figure 27 already presented the user widget for the establishment of the connection to a desired COM port. As explained before, most of the protocol definition has no impact on the software handling but is implemented in the program itself.

The process of sending and receiving messages via serial communication is an automated process which reacts to the GUI buttons initiating the connection and which pursues the stimulation sequence. This way, a wrong sequence of messages sent to the MSP can be avoided. In general, the messages are fixed according to the purpose they serve: with regard to the communication protocol definition only the *stimulation setup* message includes varying data fields and is thus the only message type where the included data depends on the program flow. The data fields are generically filled by values picked from the GUI and the message is then sent after the occurrence of a timer event. All other messages are fully implemented in the software, as data length and operation code (and thus the resulting CRC as well) are fixed for each message type. This implementation method restricts the convertibility of the program

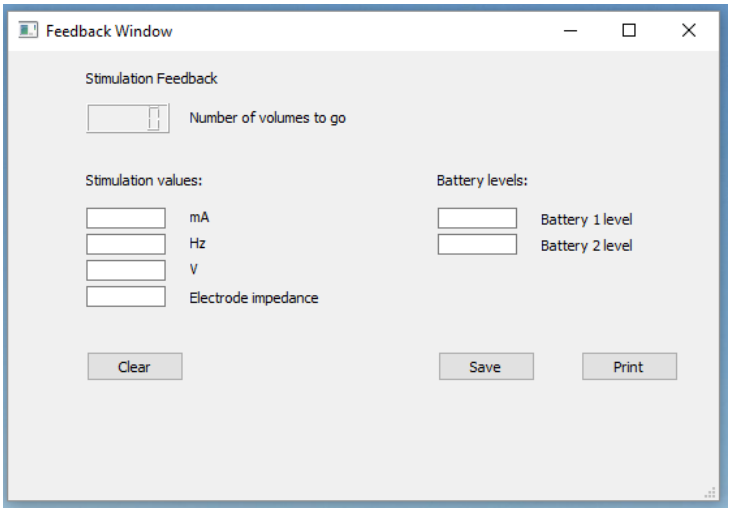

Figure 30: Graphical User Interface: Feedback window

Source: Own authorship

but provides a higher reliability and limits the error sources in the first development steps when programming this software.

In prospect for a more sophisticated second advancement of this thesis, a more generic and convertible way to implement the communication protocol would be desired.

Sending messages according to the communication protocol from PC to MSP operates through implemented serial communication via COM ports as explained before. The software accesses libraries such as the *conio.h*, *stdio.h* and *windows.h* to enable easy access to the COM ports and to use already existing functions to read from and write to the ports. The process of sending a message is simply performed by data being written to a file that actually represents the serial communication transmission buffer. This way, the data is actually sent to the communication counterpart, here the MSP.

Based on the communication protocol defining a master-slave relationship between the PC and the MSP, all messages from MSP to PC are answers to a previously sent message from the PC to MSP. This way, the PC only awaits a message after having sent one itself before. Therefore, the software reads the data arriving via serial communication at the COM port defined by the GUI. By analogy to the process of sending data, the software reads from a file which constitutes the serial communication interface when receiving data.

After a message reception, the software checks the received protocol operation code against the previously sent operation code. If the wrong code is received, e.g. the received operation code is not the counterpart to the command previously sent, it is probable that the command sent was not interpreted or executed in the right way. The software then awaits

another message containing the correct operation code before executing another task. A sequence of three wrong messages received results in the abort of the program on the PC side. The communication is then terminated and the user is informed about the termination of the program. In case of no ongoing connection between PC and MSP, the firmware times out after two seconds when no further commands are received from the PC. Thus, the whole stimulation exam is suspended.

3.5.3 SOFTWARE FUNCTIONALITY

The main functionalities of the developed software have already been outlined in the previous sections. This subsection focuses on the design and implementation of the software in terms of functionality and flow.

Apart from the previously described GUI and communication included in the program, the software itself holds crucial functionalities that work without direct user interaction. This includes various automated steps that correspond directly to user interaction, such as the sending of messages or saving of configuration values. Alerts and error interruptions exclusively depend on the inline processing of received data from the serial communication with the MSP. The program itself interprets the received values and visualizes them for the user as feedback values, more specifically as warnings and errors, depending on the determined data range.

It is not possible to totally divide the GUI from the other parts of the software. Both user interaction and the automated software are strongly interconnected. Anyhow, the following part depicts the underlying software structure and functionality.

Within the sequence of the stimulation program, the GUI performs the interaction with the user while the underlying software executes all other functions such as:

- Copying the configuration data from GUI,
- Mounting the configuration protocol,
- Being the timer for configuration set up, request, start and halt,
- Checking responses,
- Receiving the protocol,
- Processing received data,
- Showing feedback.

The stimulation values set in the GUI are saved within the software to mount the configuration protocol for the first and all following stimulation characteristics. The correct sequence and time intervals are crucial when sending the requests for feedback, the *start* and the *halt* command.

As the program contains time sensitive features such as the sequence of messages at distinct moments within the program sequence, it uses timers to guarantee this function. For this purpose, the Qt plug-in for Visual Studio provides the class QTimer. As Qt adapts to the underlying operating system, the time accuracy also depends on the supported resolution of the operating system. Most operating systems provide a resolution of approximately 1 millisecond which is enough for the demands of this thesis. Still, in many real-time situations the QTimer does not guarantee this resolution (QT DOCUMENTATION, QTIMER CLASS, 2015). The laboratory tests conducted during the development have shown that the timer resolution meets the thesis' requirements.

Four QTimers are being used during the course of the software program. A *requestTimer* expires every two seconds. This time out interval is determined by visualization requirements. When the timer expires the software sends a data request to the MSP and awaits a response. The *haltTimer* is set only once. After determining the total examination time, containing both stimulation time and time of rest, the timer is set to this period of time so that after its expiration the timer sends the *halt* command to the MSP. The *halt* command stops all remaining timers. The *startTimer* sends the *start* command after every timer expiration. It initiates the stimulation via the MSP and will only be necessary if a stimulation takes place. A period of rest must not be started. Thus, the start timer is set individually for each stimulation, determining the next interval during which no new *start* command occurs, either because of an ongoing stimulation or because of a period of rest. The *setupTimer* initiates the transmission of the configuration data. For hardware reasons, the preparation of the stimulus configuration needs a head start of at least 100 ms. The software implements this need with a time difference of 1 s previous to sending the *start* command. A brief overview about the timer functionality of all four timers is given in figure 31.

On the left hand side the time line is presented. It does not show real time intervals but different time points within the stimulation process, such as when the stimulation configuration is done and when the MRI trigger is detected. The moment of the trigger is crucial because a synchronous operation of MRI and GVS must be guaranteed to obtain useful image data. In this exemplary diagram, the examination ends after the *halt* command so that the time line terminates as well.

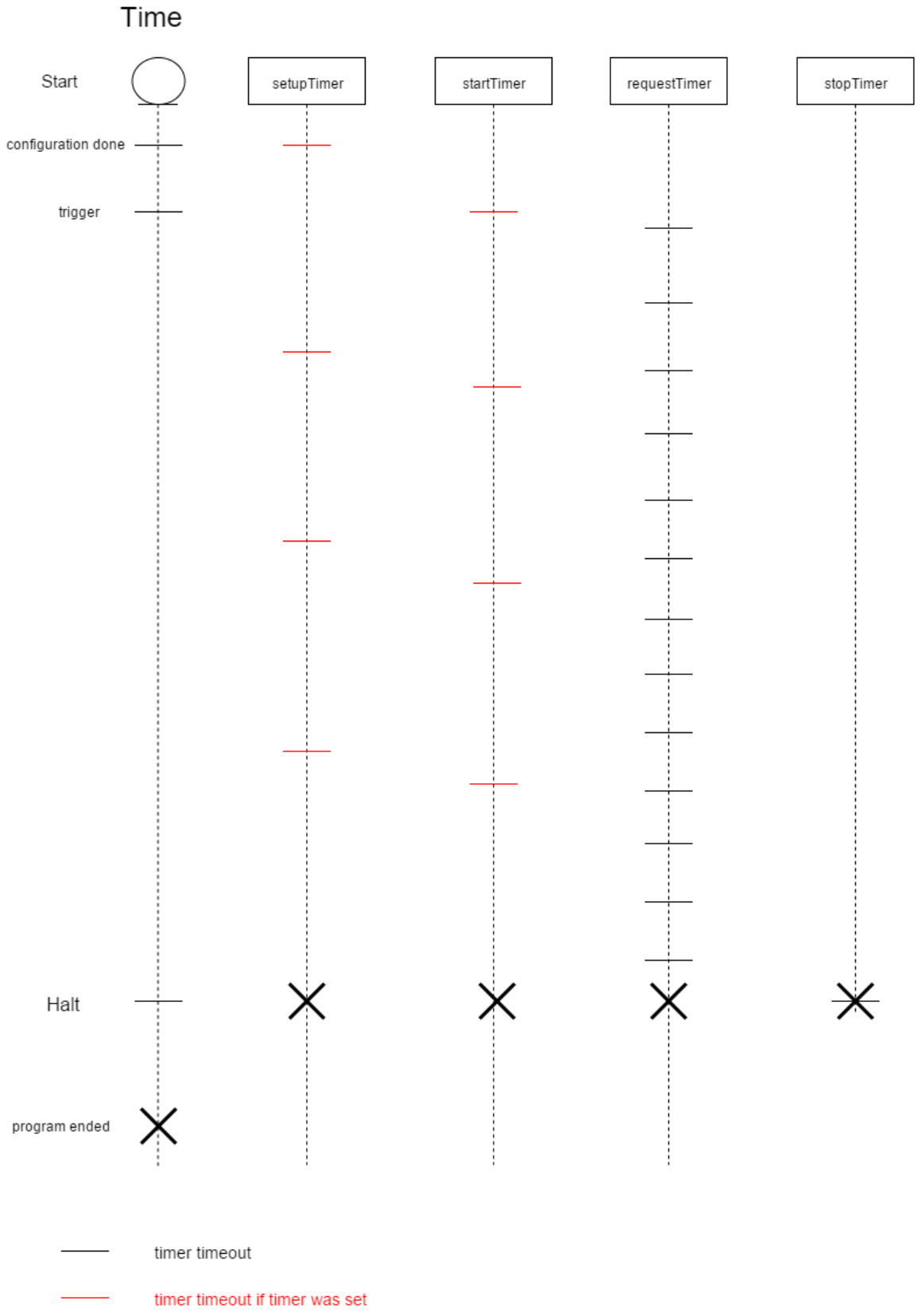

Figure 31: Diagram of the timer functionality.

Source: Own authorship

The functionality lines of the four timers are aligned parallel to the time line. Figure 31 gives an overview about the timer functionality and thus the line represents the sequence of timer time outs for each of the four timers. After every time out the timer is expected to restart, except for the *stopTimer*. Having already outlined the function of each timer, the figure solely provides a graphical overview. It can be seen that the *stopTimer* only expires once. Actually it does not even restart because of its function to determine the total stimulation time. The line of the *stopTimer* is shown on the right hand side of figure 31. Left to it, the line of the *requestTimer* is presented. The periodic expiration is shown. A time interval of 2 s can be considered for the project. The *startTimer* shown on the middle line expires synchronous after the end of one stimulation. In case of no time of rest, it directly restarts and counts until the end of the next stimulation set up. In case of an interval of rest, the red line indicates the absence of this time event. It has been outlined before that the configurations set up must be sent some time before the *start* command. This can be seen in the time line of the *setupTimer*. No configuration set up is needed in case of a rest interval. The red line again indicates the absence of this time event.

In order to ensure the ongoing flawless communication between PC and MSP, the communication protocol, which is described in subsection 3.3.3, schedules an affirmative answer from the MSP. The software checks the answer after each sent command. In case of a not acknowledged answer the previous command is sent again while in case of no received answer the communication is terminated.

During the stimulation process, the software periodically requests feedback data. In response, the MSP sends the measured values already described in subsection 3.5.1. The software extracts the data to be shown and processes the information regarding release of the patient security button or overcurrent occurrence. According to the obtained data and extracted information, the results are shown in the feedback window of the GUI and in case of errors a separate window alerting the user appears on the screen.

4 RESULTS AND DISCUSSION

Following the design and development steps, various tests must be conducted to review the functionality of all parts: hardware, firmware and software. In the course of the development, many simulations have already taken place to guarantee a flawless function not just in theory but in practice as well. Before verifying the thesis' performance in the desired fMRI environment, the conjunction of hardware, the contained firmware and software are being tested in the laboratory. These laboratory tests are outlined in section 4.1. The first tests are conducted neither with a patient nor within the MRI room. That way, the behavior especially of the current source can be tested without any health and safety implications for the patient. The second tests are conducted with two asymptomatic subjects, still not within the MRI room. These tests evaluate the safety of the subjects and evaluate the measurement of the subject's impedance.

Afterwards, this chapter outlines the discussion of the test results in section 4.2. A validation and evaluation of the project development is conducted in the following chapter 5.

4.1 LABORATORY TESTS

This chapter describes the testing steps conducted before the actual utilization of the device within a fMRI examination. It is a crucial part of the project development as the design, especially of the hardware, requires various reviews and checks before being able to put into practice what has been theoretically designed.

The laboratory tests verify the functionality in practice to enable an application on the patient. They not only validate the circuitry and thus the hardware but also the adequate communication between PC and MSP and the overall function of those two programs. A detailed description of the laboratory tests and its results are shown here. As both firmware and software are already being tested regularly during the development process, this section especially focuses on the laboratory tests of the hardware.

The following figure 32 presents an experimental setup of the prototype PCB. The experimental setup uses a voltage source instead of batteries to constitute the voltage supply. A voltage source thereby guarantees a fixed supply voltage without the need to consider the battery discharge. The circuitry provides various functions to be verified with the laboratory tests and

thus there are different experimental setups. Figure 32 shows the setup testing the protection circuit when applying a current to the patient. For this purpose, the current is provided by a signal generator instead of using the included current source which could introduce errors.

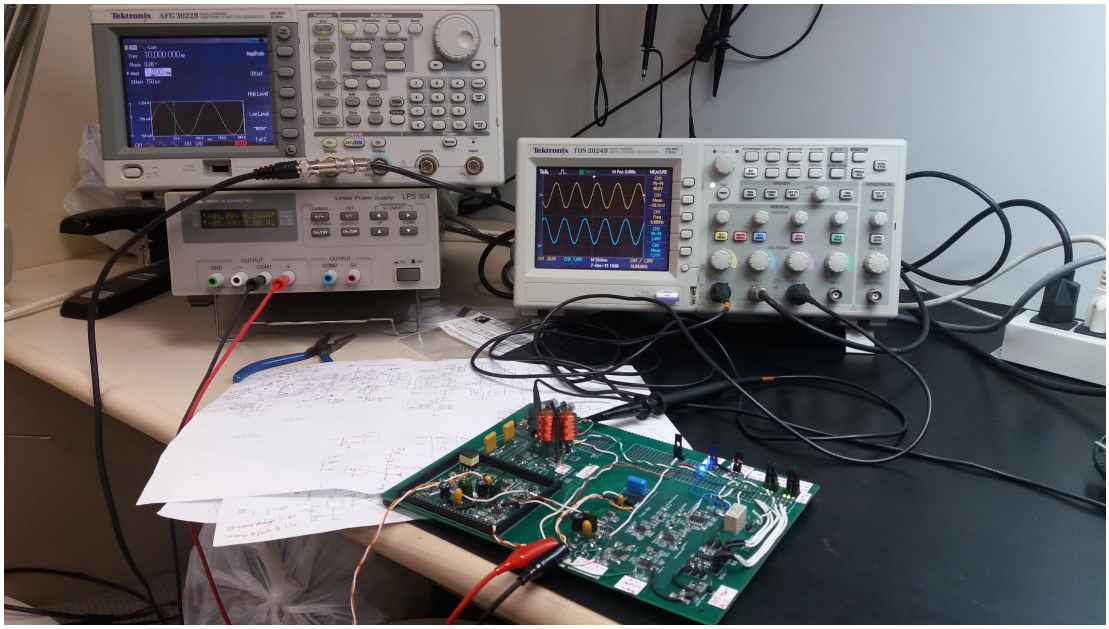

Figure 32: Experimental setup of the prototype PCB with signal generator and voltage supply via voltage source instead of battery mode.

Source: Own authorship

Figure 33 provides a close-up on the PCB board prototype used for the laboratory tests. The tests are still conducted utilizing the prototype in connection with the MSP evaluation board instead of the end product which already includes the MSP on the PCB. Still, the tests have confirmed the hardware design and have defined the last MSP output pins that are used within the hardware so that the evaluation board has provided more flexibility.

Testing the protection circuit, a special focus lies on the protection relay. Before turning on the circuitry, the two MSP output pins driving the relay set and reset must be set to Low. After turning on the whole circuit, setting the output pin to High the relay is caused to short-circuit the output of the current source so that no current is being applied to the patient. To be able to apply current to the patient, the same output pin must be driven to Low and the other output pin must pulsate to High for two or more seconds to reset the relay. Hence, the current is again applied to the patient. The possibility to short-circuit the current in case of an emergency through the set output pin is thus given. Setting the relay during the emergency is done by the comparator measuring the applied current without intervention of the MSP. The stimulation is then terminated so that the possibility to reset is given as it is important to start a new examination. This function was tested in the laboratory tests.

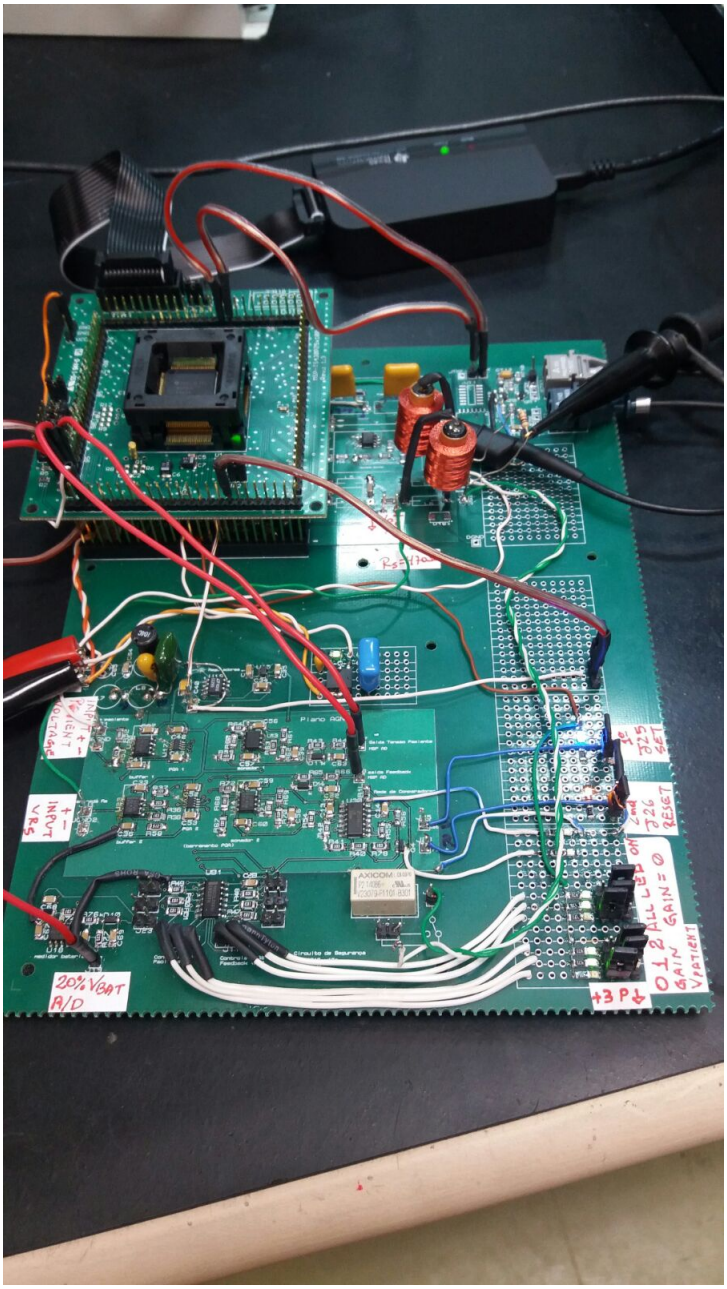

Figure 33: Close-up on the prototype of the PCB containing the current source and the protection circuit.

Source: Own authorship

The following table 4 presents the results from the voltage measurement over the patient resistor without any current over the shunt resistor. The resistance value equals 10 kΩ. The frequency of the applied currents is equal to 10 Hz. During the examination the frequency should equal no more than 5 Hz, but the oscilloscope requires a minimum frequency of 10 Hz to be able to sample data.

The determined maximum current to be applied to the patient is 5 mA (see

V_{in} (DAC)	V_{out} (R_s)
3 [V_{pp}]	60.8 [V_{pp}]
2.5 [V_{pp}]	51.2 [V_{pp}]
2.4 [V_{pp}]	46.4 [V_{pp}]
2.08 [V_{pp}]	40.8 [V_{pp}]
1.56 [V_{pp}]	31.2 [V_{pp}]
1.04 [V_{pp}]	20.4 [V_{pp}]
0.56 [V_{pp}]	10.4 [V_{pp}]
0.32 [V_{pp}]	5 [V_{pp}]

Table 4: V_{in} is the peak-to-peak amplitude generated by the MSP DAC. It is clamped on a DC level of 1.5 V. V_{out} is the peak-to-peak amplitude of the signal measured across a 10 kΩ resistor, that simulates the subject. It can be observed that an amplitude of 3 V_{pp} at the DAC output, the maximum current obtained is 6.08 mA_{pp} or 3.04 mAp.

Source: Own authorship

(MANCZAK, 2012)). As shown in table 4 considering the resistor value of 10 kΩ, the maximum input voltage of 3 V_{pp} results in a current amplitude of 6.08 mA_{pp}. Figure 34 shows a screen-shot of the oscilloscope measurement with an input voltage of 2.4 V_{pp} and its resulting output voltage across the patient resistor of 10 kΩ.

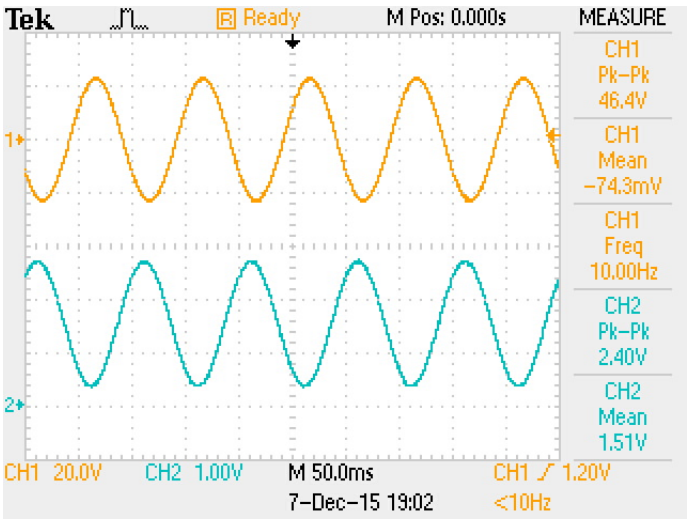

Figure 34: Screen shot of the oscilloscope measurement of the maximum input voltage. Channel 1 represents the output voltage across the 10 kΩ resistor simulating the subject while Channel 2 represents the input signal, generated with a Tektronix function generator.

Source: Own authorship

Table 5 presents the voltages over patient resistor and the shunt resistor with a value of 470Ω.

Figures 34 and 35 as well as tables 4 and 5 were obtained during the first laboratory

V_{in}	V_{outpat}	V_{outrs}
3.12 [V_{pp}]	60.8 [V_{pp}]	5.12 [V_{pp}]
2.56 [V_{pp}]	51.2 [V_{pp}]	4.32 [V_{pp}]
2.16 [V_{pp}]	40.8 [V_{pp}]	3.52 [V_{pp}]
1.68 [V_{pp}]	30.8 [V_{pp}]	2.56 [V_{pp}]
1.12 [V_{pp}]	20.4 [V_{pp}]	1.76 [V_{pp}]
0.52 [V_{pp}]	10.4 [V_{pp}]	0.94 [V_{pp}]

Table 5: V_{in} is the voltage at the MSP ADC output and V_{out} is the voltage across a 10 kΩ resistor, simulating the patient. The input voltage V_{in} is clamped at a 1.5 V DC level. The first line shows that the maximum V_{in} that can be provided by the DAC of the MSP is 3.12 V_{pp}. The resulting voltage across the patient resistor was determined to be 60.8 V_{pp} and the voltage across the shunt resistor was determined to be $_{pp}$.

Source: Own authorship

tests, where the subtracter and adder circuit had a gain of 2.2 and the shunt resistor had a value of 470 Ω.

The following figure 35 exemplary presents a screen shot of the oscilloscope display of the output voltages over patient and shunt resistor. The blue line shows the input voltage, the purple line the voltage over the shunt resistor and the yellow line the voltage over the patient resistor.

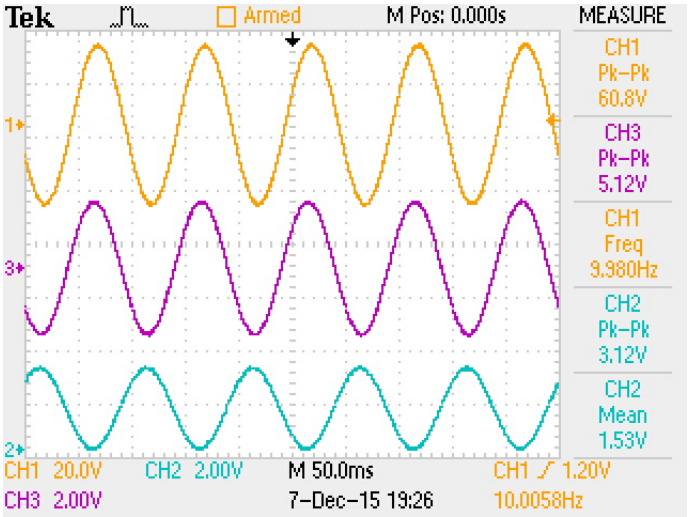

Figure 35: Screen-shot of the oscilloscope measurement of output voltages over patient resistor and shunt resistor. Channel 2 represents the input voltage, Channel 1 represents the output voltage over the patient resistor and Channel 3 represents the output voltage over the shunt resistor.

Source: Own authorship

The following part of this section shows the signal amplitude and frequency at distinct

parts of the circuitry. Laboratory tests confirmed the flawless functionality of the DAC, ADC, PGAs and the firmware that controls the ICs named before. However, for these second tests the gain of the subtracter and adder circuit was increased to allow a larger signal amplitude at the current source input, providing a peak current amplitude of 5 mA, in other words a peak-to-peak current amplitude of 10 mA. Also, the shunt resistance was reduced to 270 Ω (before, it has been 470 Ω) to avoid that the R_s signal amplitude exceeds 3 V_{pp}. The limit of a 3 V_{pp} amplitude for the measured signal is determined by the maximum input voltage at the ADC of the MSP.

Figure 36 presents the voltage signal observed in the current source circuit. The signal is adjusted to a sine wave of 1 V_{pp} and a mean value of 1.5 V by the Tektronix Function Generator (shown as blue line in figure 36). A 10 kΩ resistor is used as the current source load, simulating the patient. The generated signal is then applied to the signal conditioning circuit input (J2). It can be seen that the ratio of the voltage measured across the shunt resistor of 270 Ω, placed in series with the 10 kΩ resistor (shown as orange line in figure 36) and the voltage measured at the current source input (Js), after the signal conditioning circuit, is approximately equal to one.

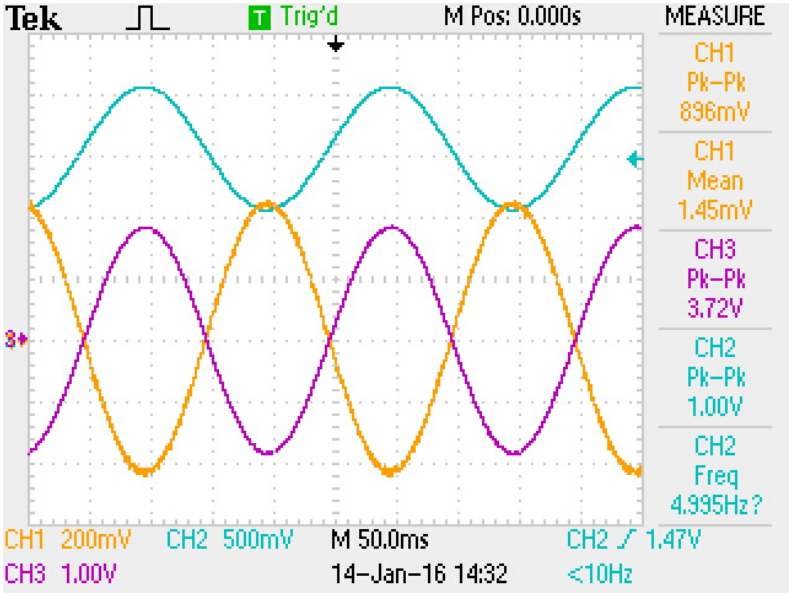

Figure 36: Voltage signals observed in the current source circuit. Input signal generated by the Tektronix Function Generator. Blue line (J2): Tektronix Function Generator Input signal, 1 V_{pp} and mean value of 1.5 V. Purple line (J_S): Signal applied at the current source input, 3.72 V_{pp} and mean value of 0 V. Orange line (J_{R1}): Voltage across V_{Rs}, 0.9 V $_{pp}$ and a mean value of 1.45 V (R_S = 270 Ω).

Source: Own authorship

The next figure 37 presents the measured voltage signal at the monitoring circuit. The

input signal is generated by the Tektronix Function Generator to a sine wave of 1 V_{pp} and a mean value of 1.5 V (blue line). The voltage across R_s is shown in the orange line. The amplitude is approximately 1.74 V_{pp} and the DC value is nearly 0 V. The purple line represents the conditioned signal with a DC level of 1.5 V to be applied to the ADC of the MSP.

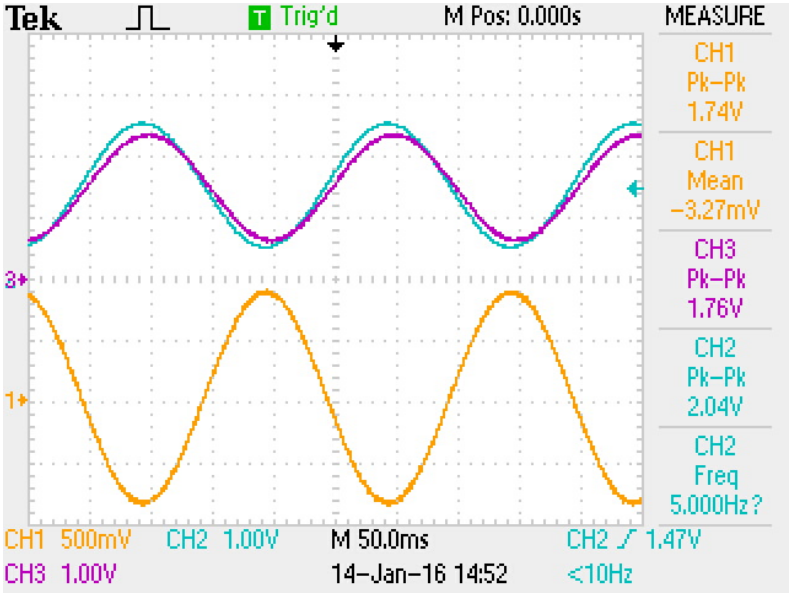

Figure 37: Voltage signals measured in the current monitoring circuit. Blue line: Input signal, sine wave of 1 V_{pp} and a mean value of 1.5 V. Orange line:Voltage across R_S, amplitude 1.74 V_{pp} and a DC value near 0 V. Purple line: Conditioned signal, DC level adjusted to 1.5 V.

Source: Own authorship

To confirm the correct functionality of the MSPs DAC, the laboratory tests have executed the same tests with the input signal being generated by the DAC and controlled by the firmware. This is shown in figure 38. The input signal is being configured to a sine wave of 1.1 V_{pp} with a DC value of 1.5 V and a frequency of 5 Hz (blue line). The voltage measured across the shunt resistance is 980 mV_{pp} and and a DC value near zero. The conditioned signal with a DC level adjusted to 1.5 V and an amplitude of 2.56 V_{pp} is then applied to the ADC of the MSP. Figure 38 presents the measured values.

Figure 39 shows the signals measured in the signal conditioner. It is designed to monitor the voltage applied to the subject and provided by the current source. The patient is simulated through a resistor of 10 kΩ. The signal applied to the patient, here shown as the orange line in the figure, has an amplitude of 33.6 V_{pp} and a mean value of approximately 0 V. As an input of the signal conditioning circuit, a sample of the 33.6 V_{pp} with a mean value of 0 V is obtained by a resistor divider of $\frac{5.1k\Omega}{(100k\Omega+5.1k\Omega)}$. The output of the signal conditioning circuit is a signal with a mean value of approximately 1.5 V and an amplitude of 1.64 V_{pp}. During the data acquisition the PGA was set to a gain of 1. The input signal of the current

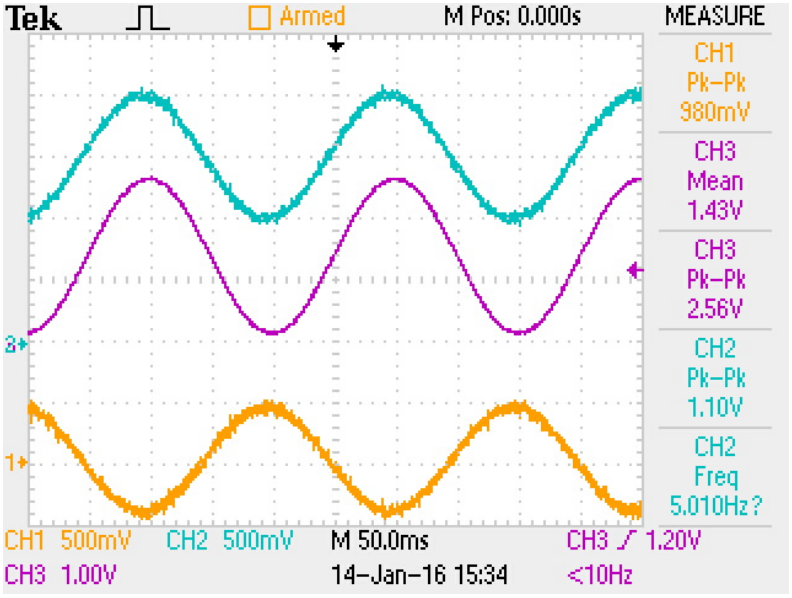

Figure 38: Voltage signals measured in the current monitoring circuit with an input signal provided by the DAC. Blue line: Input signal, 1.1 V_{pp} amplitude with DC value of 1.5 V and 5 Hz frequency. Orange line: Voltage across R_S, 980 mV_{pp} amplitude and a DC value of 0 V. Purple line: Conditioned signal, 2.56 V_{pp} and a DC value of 1.5 V.

Source: Own authorship

source is provided by the Tektronix Function Generator which generates a sine wave of 1 V_{pp} with a mean value of 1.5 V.

The next figure 40 presents the laboratory tests measuring the voltage across the simulated patient and the shunt resistor where the feedback measurement is done. The blue line again shows the current source input, a sine wave with an amplitude of 1 V_{pp} and a mean value of 1.5 V. The voltages are measured across a resistor with the value of 10 kΩ, simulating the patient, and across the shunt resistor with 270 Ω resistance. The voltage measured across the patient has an amplitude of around 34.4 V_{pp} and a mean value near 0 V while the voltage across the shunt resistor only has an amplitude around 1 V_{pp} and also a mean value near 0 V.

The voltages measured at the positive and negative output of the flyback IC are found to be +/- 40 V. The presence of a ripple is observed. This is due to a neglection in the development of the current source as the voltage multiplier (MAX1682) does not provide the current output which is pushed by the flyback component. This results in an overcurrent at the voltage multiplier output that can be experienced at the flyback output as a ripple over the positive and negative output voltage. The measured output voltages are presented in figure 41.

Figures 36 to 40 present all important signals that are measured within the course of the circuitry.

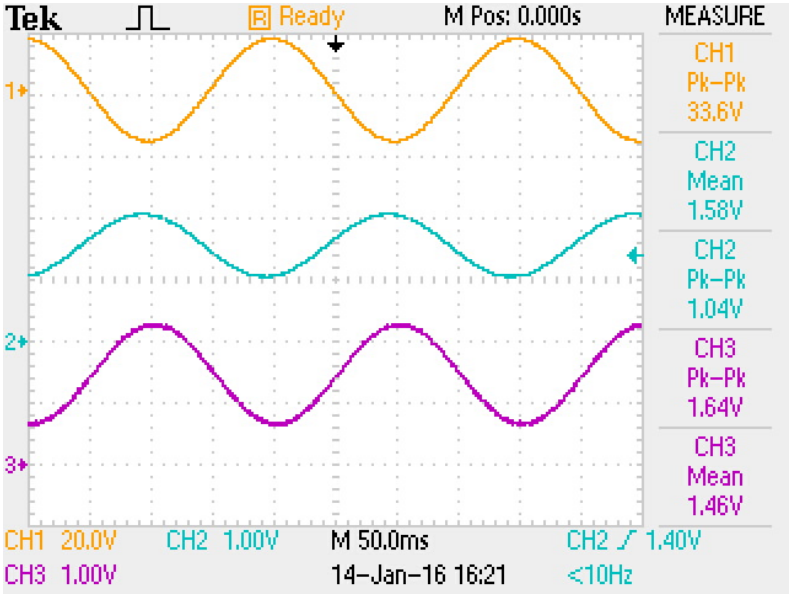

Figure 39: Voltages measured in the signal conditioning circuit. Blue line: Sine wave generated by the Tektronix Function Generator, 1 V_{pp} amplitude and a mean value of 1.5 V. Orange line: Signal applied to the patient, amplitude of 33.6 V_{pp} and a mean value near 0 V. Purple line: Output of the signal conditioning circuit, amplitude of 1.64 V_{pp} and a mean value of approximately 1.5 V.

Source: Own authorship

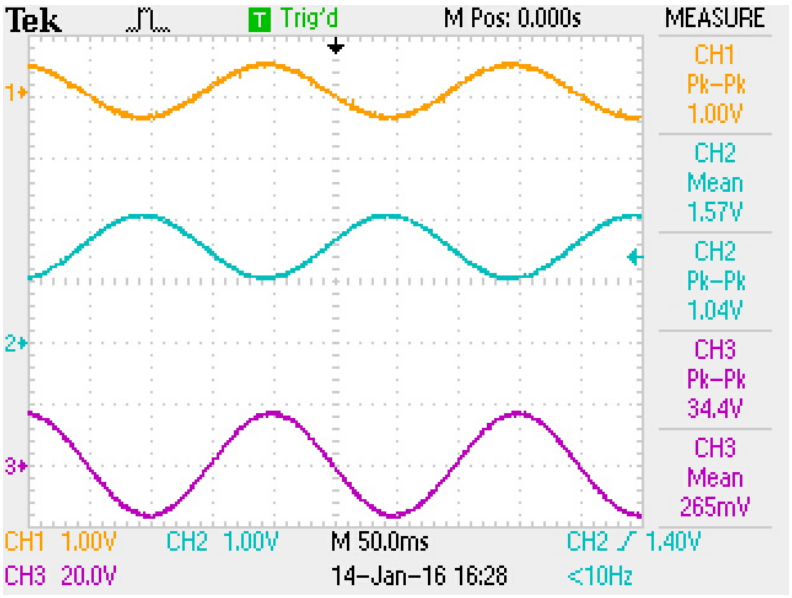

Figure 40: Blue line: Current source input signal, sine wave with an amplitude of 1 V_{pp} and a mean value of 1.5 V. Orange line: Signal measured across the shunt resistor, 1 V_{pp} amplitude and a mean value near 0 V. Purple line: Signal measured across the patient resistor, 34.4 V_{pp} amplitude and a mean value near 0 V.

Source: Own authorship

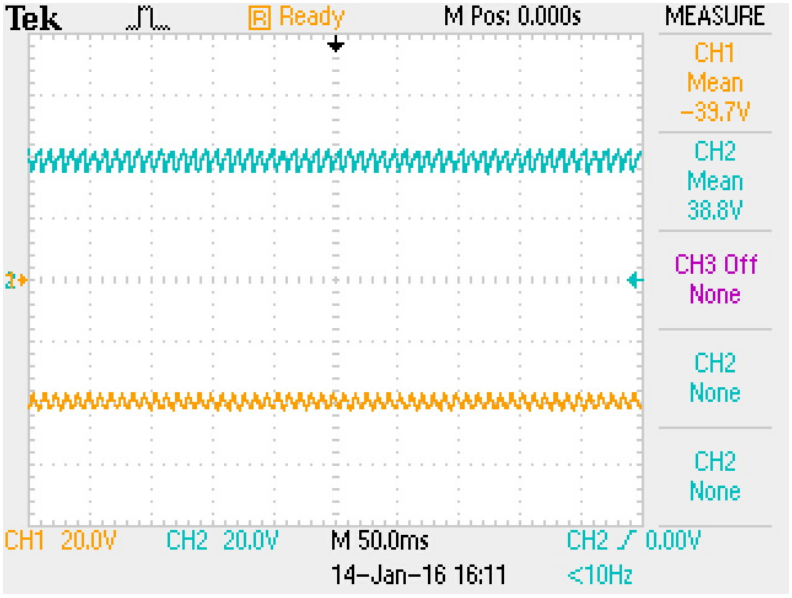

Figure 41: Positive and negative output of the flyback IC.

Source: Own authorship

Subsequently, *in vivo* tests were performed to evaluate the behavior of the electrical current source with two asymptomatic subjects, later referred to as subject #1 (age: 54 years, height: 1.69 m, weight: 77 kg) and subject #2 (age: 22 years, height: 1.82 m, weight: 90 kg). Rubber silicone electrodes were used to apply the adjusted current. They were placed above the mastoid processes and fixed with 3M Micropore. In order to reduce the electrical impedance between the subjects skin and the silicone electrodes, an electrically conductive gel was applied on the skin before attaching the electrodes.

To determine the impedance of the subject, the voltages are measured; first across the shunt resistor and second across the series connection of shunt resistor and subject. The shunt resistance is known to be 270 Ω. The subject's impedance can be determined through the following equations:

$$I = \frac{U_s}{R_s}$$

The current applied to the patient can be determined through the fraction of the voltage across the shunt resistor and the shunt resistance. As shunt resistor and subject are mounted in series, the current through the shunt resistor is the same as the current through the subject. The voltage across the subject can be determined as the difference between the voltage across both shunt resistor and subject and the voltage across the shunt resistor.

$$U_p = \frac{U_{sp}}{U_p}$$

Finally, the impedance is calculated as the fraction of the voltage across the subject

and the total current applied.

$$Z_p = \frac{U_p}{I}$$

The succeeding figure 42 presents the *in vivo* test results with subject #1 for a stimulation current configured as a sine wave with an amplitude of 1.5 mA_p and a frequency of 1 Hz. The measured voltage across the resistors R_p and R_s, constituting the current source output, equals 23.6 V_{pp}. The measured voltage across the shunt resistor, with a resistance value of 270 Ω, equals 680 mV_{pp}. The subject's impedance can thus be calculated as 9.37 kΩ.

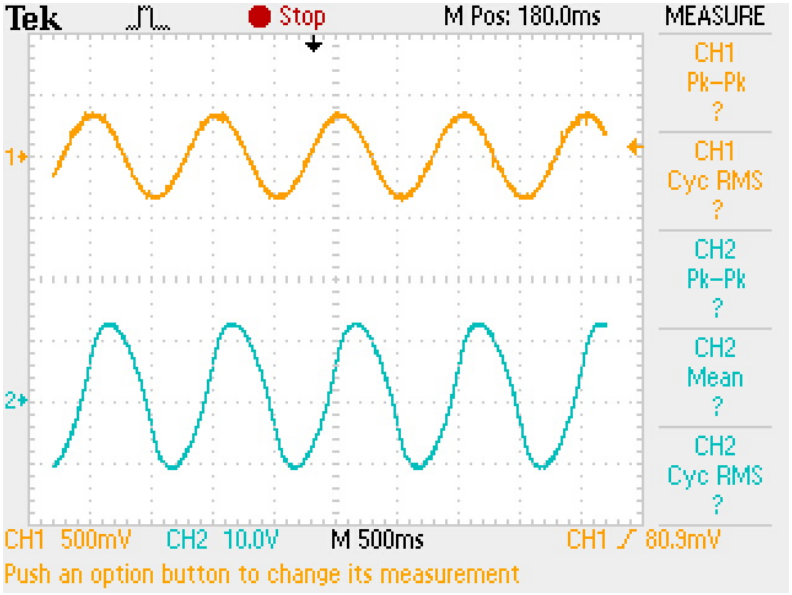

Figure 42: *In vivo* test with an asymptomatic subject #1. Current parameter configuration:Sine wave, amplitude 1.5 mA_p, frequency: 1 Hz. Blue line: Voltage across R_p and R_s. Orange line: Voltage across R_s.

Source: Own authorship

Below, figure 43 presents the *in vivo* test results of the second test with subject #1 for a stimulation current configured as a sine wave with an amplitude of 2 mA_p and a frequency of 1 Hz. The measured voltage across the resistors R_p and R_s equals 28.8 V_{pp}. The measured voltage across the shunt resistor equals 960 mV_{pp}. The subject's impedance for this test is thus calculated as 8.10 kΩ.

Figure 44 presents the *in vivo* test results with subject #2 for a stimulation current configured as a sine wave with an amplitude of 1.5 mA_p and a frequency of 1 Hz. The measured voltage across the resistors R_p and R_s equals 27.2 V_{pp}. The measured voltage across the shunt resistor equals 680 mV_{pp}. The subject's impedance is calculated as 10.8 kΩ based on the measured data.

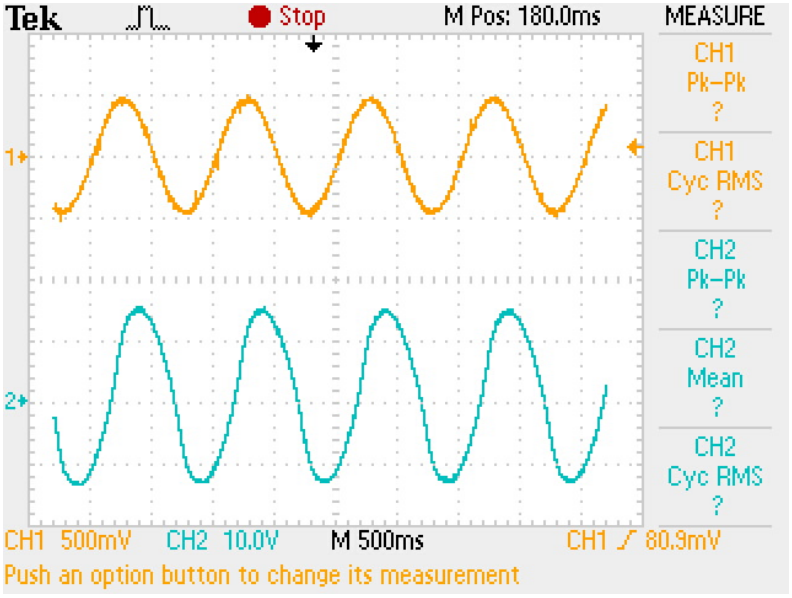

Figure 43: *In vivo* test with an asymptomatic subject #1. Current parameter configuration: Sine wave, amplitude 2 mA_p, frequency: 1 Hz. Blue line: Voltage across R_p and R_s. Orange line: Voltage across R_s.

Source: Own authorship

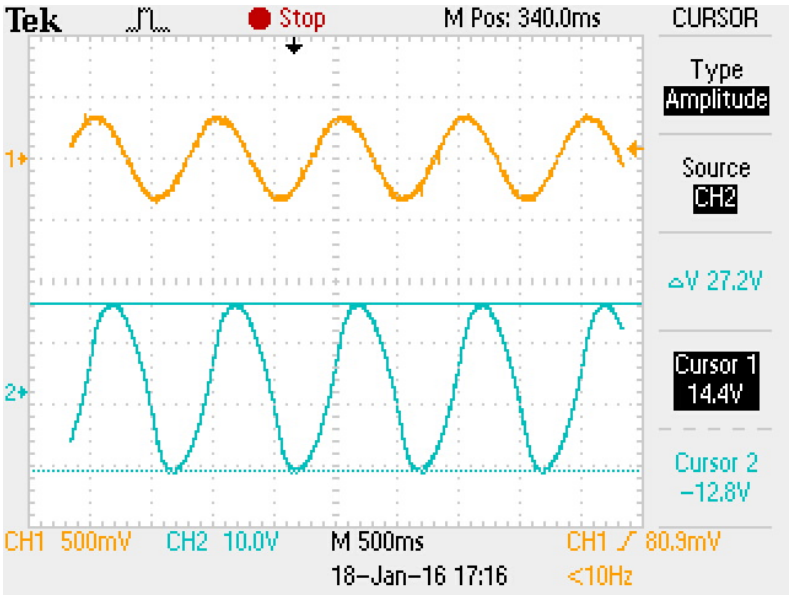

Figure 44: *In vivo* test with an asymptomatic subject #2. Current parameter configuration: Sine wave, amplitude 1.5 mA_p, frequency: 1 Hz. Blue line: Voltage across R_p and R_s. Orange line: Voltage across R_s.

Source: Own authorship

The following figure 45 presents the test results of the second *in vivo* test with subject #2 for a stimulation current configured as a sine wave with an amplitude of 2 mA_p and a frequency of 1 Hz. The measured voltage across the resistors R_p and R_s equals 40.8 V_{pp}.

The measured voltage across the shunt resistor equals 920 mV_{pp}. The subject's impedance determined through the *in vivo* tests can thus be calculated as 11.97 kΩ.

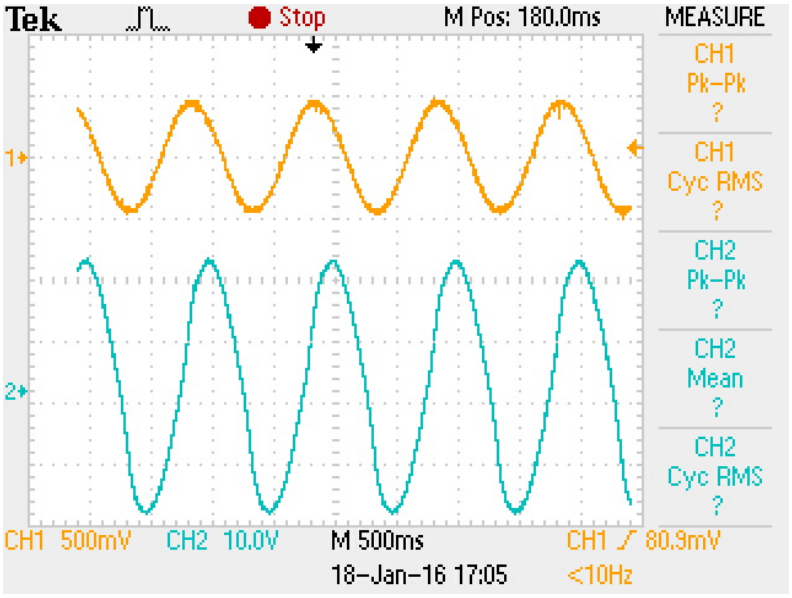

Figure 45: *In vivo* test with an asymptomatic subject #2. Current parameter configuration: Sine wave, amplitude 2 mA_p, frequency: 1 Hz. Blue line: Voltage across R_p and R_s. Orange line: Voltage across R_s.

Source: Own authorship

Figures 42 to 45 show that there is a small difference between the current adjusted in the firmware and the current actually applied to the patient. This problem can be solved by adjusting the current generation of the MSP. It can be seen that the voltage across R_p and R_s is slightly disfigured but still represents a sine wave. Figure 46 presents the test results of a third *in vivo* test with subject #2 for a stimulation current configured as a sine wave with an amplitude of 1.5 mA_p and a frequency of 1 Hz. The measured voltage across the resistors R_p and R_s equals 39.2 V_{pp}. The measured voltage across the shunt resistor equals 660 mV_{pp}. Thus, the subject's impedance determined through the *in vivo* tests has been calculated as 16.04 kΩ.

The determined subject impedance presents a value much higher than the values calculated before. This is due to an electrode remaining slightly loose from the skin which causes the impedance to rise. Section 4.2 outlines the possibility to use this behavior to check the electrical connection during the fMRI studies. The importance of the detection of loose electrodes in order to prevent an increase of pain is also explained there.

The laboratory tests are now complete and an evaluation of the stimulator functionality can be based on the results obtained. The discussion of the test results is presented in the following section 4.2.

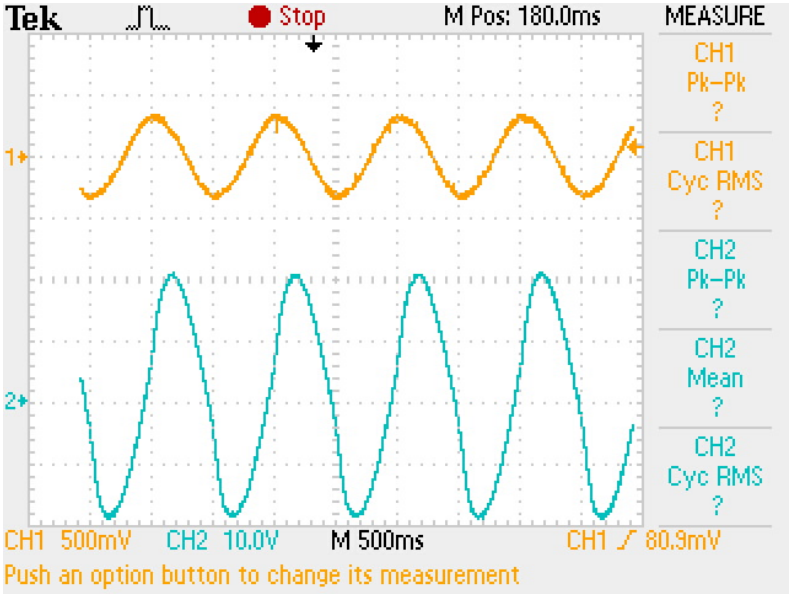

Figure 46: *In vivo* test with an asymptomatic subject #2. Current parameter configuration: Sine wave, amplitude 1.5 mA_p, frequency: 1 Hz. Blue line: Voltage across R_p and R_s. Orange line: Voltage across R_s. Obs.: The right electrode was slightly loosened from the skin.

Source: Own authorship

4.2 DISCUSSION

This section discusses the results of the previously presented data and the thereby acquired data. The first laboratory tests have been conducted without a patient who has been simulated through a resistance of 10 kΩ. At this point of the thesis no statement concerning the function within the MRI can be made as no such tests were conducted. The project design aims at low to no EMI and RFI for the galvanic stimulator but this has not been proven yet. Moreover, the continuation of high image quality must still be shown in fMRI tests. The function of proper trigger detection and synchronization with the MRI device will be examined in further tests.

The evaluation of the protection circuit is positive. An electrically correct function has been shown in tests by setting and resetting the relay through MSP and the proper stimulation signal. The electrical circuit of the patient button has been shown to react in a correct measure, guaranteeing the patient's safety.

The hardware tests not only stated the proper functionality of the circuitry but also helped fixing problems (such as the gain of operational amplifiers) or helped configuring the MSP pins responsible for distinct functions (for example the configuration of the PGAs, the DAC, etc.). The signal flow within the circuitry was checked with signals generated by the Tektronix Function Generator and generated by the DAC output of the MSP. That way, in a

first step the required voltages could be determined so that the MSP later provided the correct anticipated signal amplitude. The laboratory tests checked distinct points of the circuit, such as the flyback outputs, the signal conditioning circuit, both the ADC and DAC conversion and finally the measurement of the voltage across patient and shunt resistor. The latter provides information about the stimulation state and the feedback values.

The laboratory tests with two asymptomatic subjects confirmed the assumed patient impedance of approximately 10 kΩ. The measured values ranged between 8.10 kΩ and 11.97 kΩ for proper attachment of the electrodes. During the last examination - the results shown in figure 46 - the right electrode remained slightly loose and unattached to the skin. The impedance value then increased by nearly 50% in comparison to the other impedance values obtained. This test confirms that it is possible to check the electrical current between the electrode and the skin through a determination of the impedance. An increased impedance points to loosened electrodes which might reduce the amount of contact between the electrode and the skin. This increases the current density and thus the feeling of pain experienced by the subject. Previous research by Manczak and Della Justina has shown that galvanic vestibular stimulation can induce the experience of pain and skin burns in the area where the electrodes are placed on the skin (MANCZAK, 2012) (JUSTINA, 2014). Normally the subject itself would complain about the increase of pain which might cause injuries like burns to the skin. Still, sometimes the subject does not complain and interprets the occurrence of pain as normal. Thus, it is important that a loose contact of the electrodes is detected even without the subject complaining about discomfort. The laboratory tests with asymptomatic patients confirmed the possibility to detect an increased impedance which can be used as a prevention from pain and injuries due to heat dissipation.

The communication between the PC and the MSP has been tested while developing both firmware and software. The requirements towards GUI and both firmware and software functionalities to conduct the galvanic vestibular stimulation examination are met, even if some modifications are planned as a thesis prospect. During the laboratory tests, the software and firmware have already been used to configure and generate the stimulation current. Their correct behavior was confirmed during all tests. A comparison between the stimulation current generated by the Tektronix Function Generator and generated by the DAC of the MSP showed that the signal behavior at distinct parts of the circuit is the same.

Summing up, the conducted tests confirmed the design of the three project parts, being hardware, firmware and software. Necessary alterations have been made regarding the configuration and dimensioning of distinct parts of the thesis so that fMRI tests are expected to

be successful and also to confirm the initial hypothesis that the here designed GVS can be used in fMRI exams. The following chapter 5 outlines the conclusion of this master thesis.

5 CONCLUSION

fMRI examination can be used to map activated brain areas to a somatosensory stimulus as this procedure detects the increase of oxygenated blood flow which is linked to the number of neurons that are activated. fMRI exams are a method of choice when analyzing the vestibular system. Literature depicts two main possibilities to stimulate the human vestibular system, caloric and galvanic stimulation, although galvanic stimulation is suggested for vestibular stimulation within the fMRI (LOBEL et al., 1998). The main advantages of galvanic stimulation over caloric stimulation are that the electrical current is easier to be configured, controlled and reproduced than a caloric stimulus (LOBEL et al., 1998) (BENSE et al., 2001) (STEPHAN et al., 2005).

Even with the number of articles concerning this research topic increasing, there is still no device available to conduct an examination with. A former master thesis described the development of a galvanic vestibular stimulator (MANCZAK, 2012) which has been used in a PhD thesis investigating the relationship between the visual and vestibular system (JUSTINA, 2014). This master thesis implements a further development of the galvanic vestibular stimulator designed by Manczak et al. in 2012 and restructures the circuit design especially by adding a microcontroller as the heart of the control unit. Some new functionalities such as the feedback measurement or the battery monitoring are added in order to enhance the performance of the GVS.

One of the main ideas when deciding to enhance the former GVS device was to integrate digital components to the hardware part that is placed in the fMRI under the hypothesis that this would not interfere with the image quality of the fMRI exam.

The requirements of the device are related to the fMRI setting which includes radio frequency pulses and a strong magnetic field with strong magnetic gradients. Thus, the hardware must be protected from RFI and EMI which might even destroy the components or at least induce interference signals. During the whole stimulation process, the safety of the subject must be ensured both by firmware and by hardware. A relay has been integrated in the circuit to prevent an overcurrent to the subject. Circuitry monitoring the voltage across the patient detects the feedback and can thus alert the user (who is conducting the examination) if the patient protection button is released or if the subject's impedance increases due to the loosening of one of the electrodes.

The voltage supply of the current source that follows the topology of a Howland current pump is given by an IC of flyback topology providing a voltage of +/- 67.5 V which enables a maximum stimulation current of 4.5 mA_p.

The firmware running on the microcontroller that controls the hardware that is placed in the MRI room assumes all control functions and runs the pins responsible for enabling the circuitry, adjusting the stimulation configuration, measuring all relevant data and guaranteeing the safety of the subject. Therefore, peripheral parts of the microcontroller such as the DMA, DAC and ADC are used. To communicate with the software that allows user interaction through the GUI, optical communication was established via LEDs, photo diodes and fiber optic cables. The communication protocol was determined to allow flawless communication of the master-slave topology, where the PC constitutes the master and the microcontroller constitutes the slave. The optical communication presents the sole interface between PC and microcontroller respectively between software and firmware. The software basically provides an interface for user interaction and then sends the commands to the firmware in order to control the stimulation.

The GVS has been tested in the laboratory. The first tests evaluated the generation of the stimulation signal through the course of the hardware circuit until being applied to a resistor simulating the subject's impedance. Later, the actual stimulation current has been applied to two asymptomatic subjects. All tests showed the proper functionality of the device.

The hypothesis that the new concept of the hardware circuit will neither decrease the image quality nor experience interfering signals within the circuitry has not been tested yet. Until now, only the functionality of the GVS has been checked by laboratory tests. Statements concerning the fMRI validation cannot be made at this point.

6 PROSPECT

Closing the thesis description and conclusion, some of the questions asked in the beginning have not been answered yet. In the course of the thesis' design, various review steps were included to guarantee a successful outcome of the development. These review steps in conjunction with laboratory tests and hardware manufacturing consumed a lot of time and resources. Thus, the finalizing tests in the MRI room during a fMRI examination have not yet been conducted.

Until this point of the thesis development, the correct function of the device has been proven in laboratory tests and simulations. The remaining question is how the MRI device will react to the placement of the hardware inside and whether the image quality would suffer noticeably. The thesis' design is oriented to minimize the interference between GVS and MRI. Compatibility tests have been conducted in the previous research project which showed that the MR imaging is not compromised by the first generation GVS. To validate this thesis in terms of utility and impact, the fMRI compatibility tests will still have to be conducted. These tests take place as soon as the most recent hardware is manufactured and testing within the fMRI is allowed and prepared. For this purpose, an aluminum blinding box will be manufactured to enclose the circuitry, shield the RF pulses and prevent EMI.

The GVS tests are conducted with volunteers without any pathology in relation to the vestibular system as the tests verify the function and behavior of the device and are not conducted to provide a diagnosis for the patients. The volunteers and users (patients and conductors) are briefed for the adequate handling of the device. The volunteer will be instructed how to handle the patient security button, when to press and when to release it. Moreover, the conductor must be advised how to handle the user interface, which configuration to make and how to react in case of software alerts. It is crucial to know that in any case of errors, the stimulation process is stopped and that a new stimulation examination might only be started after determining the previous error source. The current stimulation shall not continue in this case. The protection circuit will prevent the volunteers from being harmed even if the device presents a malfunction. However, the user should still verify the volunteers well-being after an error occurrence, especially when the patient button has been released.

In the process of GVS tests, full stimulation sequences are tested depending on the alternation of different wave forms and rest. Low frequencies and amplitudes as well as high

frequencies and amplitudes should be investigated. Besides the GVS behavior during the fMRI examination, the image quality is the most important characteristic to rate the thesis' success and utility.

Further modifications of the firmware and software are planned subsequently to the fMRI tests. The implementation of the communication protocol will then be altered to allow a more dynamic communication and replace the fixed protocols that are implemented up to this point of the thesis. When having conducted the tests in the fMRI, the communication between PC and MSP will be settled so that modifications in the security prompt are conceivable. The communication time out could then be adjusted to real time values, being confirmed by the tests conducted.

In addition to the measurement of the subject's impedance as has been referred to in chapter 4, it might be interesting in vestibular research to determine the conclusive impedance variance that is independent of the individual. With this variance a limit for the maximum coherent impedance can be determined, which can then be included as another safety arrangement.

The GVS project will be part of a post doc thesis diagnosing and treating patients that suffer from vestibular diseases after having conducted all pending tests. This way, the thesis will continue to be in a process of alterations and modifications affecting all three parts: the hardware, the firmware and the software.

REFERENCES

AVAGO TECHNOLOGIES. **HFBR-1521Z**. [S.l.], August 2011. Last viewed 08/01/2016. Available at <http://www.avagotech.com/products/industrial-fiber-optics/industrial-control-general-purpose/650nm/hfbr-1521z>.

AW, S.; TODD, M.; HALMAGYI, G. Latency and initiation of the human vestibuloocular reflex to pulsed galvanic stimulation. **Jornal of Neurophysiology**, n. 96, p. 925–930, 2006.

BENSE, S.; STEPHAN, T.; YOUSRY, T. A.; BRANDT, T.; DIETERICH, M. Multisensory cortical signal increases and decreases during vestibular galvanic stimulation (fmri). **Journal of Neurophysiology**, vol. 85, p. 886 –899, 2001.

COHEN, B.; YAKUSHIN, S. B.; HOLSTEIN, G. What does galvanic vestibular stimulation actually activate? **frontiers in Neurology**, vol. 2, n. 90, p. 1–2, January 2012. Opinion article.

DELLA-JUSTINA, H.; GAMBA, H.; LUKASOVA, K.; SILVA, M. Nucci-da; WINKLER, A.; AMARO, E. Interaction of brain areas of visual and vestibular simultaneous activity with fmri. **Experimental Brain Research**, n. 233, p. 237–252, 2015.

DELLA-JUSTINA, H. M.; MANCZAK, T.; WINKLER, A. M.; ARAúJO, D. B. d.; SOUZA, M. A. d.; AMARO, E.; GAMBA, H. R. Galvanic vestibular stimulator for fmri studies. **Revista Brasileira de Engenharia Biomédica (Impresso)**, n. 30, p. 70–82, 2014.

DIODES INCORPORATED. **SMBJ85CA**. [S.l.], June 2009. Last viewed on 08/01/2016. Available at <http://www.diodes.com/$_{f}iles/datasheets/ds$19002.pdf¿.

FASOLD, O.; BREVERN, M. von; KUHBERG, M. e. a. Human vestibular cortex as indentified with caloric stimulation in functional magnetic resonance imaging. **NeuroImage**, n. 17, p. 1384–1393, 2002.

FITZPATRICK, R. C.; DAY, B. L. Probing the human vestibular system with galvanic stimulation. **Journal of Applied Physiology**, vol. 96, p. 2301 – 2316, 2004.

GUINAND, R.; BERG, R. van de; RANIERI, M.; S., C.; J., D.; NGUYEN, T.; MICERA, A.; STOKROOS, R.; KINGMA, H.; GUYOT, J.; FORNOS, A. P. Vestibular implants: Hope for improving the quality of life of patients with bilateral vestibular loss. In: **Conference proceedings: Annual International Conference of the IEEE engineering in Medicine and Biology Society**. [S.l.: s.n.], 2015.

JUSTINA, H. M. D. **Estudo da interação cerebral entre as áreas funcionais dos sistemas visual e vestibular**. Tese (Doutorado) — Universidade Tecnológica Federal do Paraná Programa de Pós-Graduação em Engenharia Elétrica e Informática Industrial, 2014.

KERBER, K. A.; NEWMAN-TOKER, D. E. Misdiagnosing dizzy patients: Common pitfalls in clinical pratice. **Neurologic Clinics**, vol. 33, n. 3, p. 565–575, 2015.

LINEAR TECHNOLOGIES. **LT1129-3**. [S.l.], 1 1994. Last viewed on 08/01/2016. Available at <http://cds.linear.com/docs/en/datasheet/112935ff.pdf>.

LINEAR TECHNOLOGIES. **LTC6910-3**. [S.l.], 1 2002. Last viewed on 08/01/2016. Available at <http://cds.linear.com/docs/en/datasheet/6910123fa.pdf>.

LINEAR TECHNOLOGIES. **LT8300**. [S.l.], 1 2012. Last viewed on 08/01/2016. Available at <http://cds.linear.com/docs/en/datasheet/8300f.pdf>.

LINEAR TECHNOLOGIES. **LTC6090**. [S.l.], 1 2012. Last viewed on 08/01/2016. Available at <http://cds.linear.com/docs/en/datasheet/6090fe.pdf>.

LOBEL, E.; KLEINE, J. F.; BIHAN, D. L.; LEROY-WILLIG, A.; BERTHOZ, A. Functional mri of galvanic vestibular stimulation. **Journal of Neurophysiology**, vol. 80, p. 2699 – 2709, 1998.

MACDOUGALL, H.; MOORE, S.; CURTHOYS, I.; BLACK, F. Modeling postural instability with galvanic vestibular stimulation. **Experimental Brain Research**, n. 172, p. 208–220, 2006.

MANCZAK, T. **Estimulador galvânico vestibular para fMRI**. Dissertação (Mestrado) — Universidade Tecnológica Federal do Paraná, 2012.

MARCELLI, V.; ESPOSITO, F.; ARAGRI, A. e. a. Spatio-temporal pattern of vestibular information processing after brief caloric stimulation. **European Journal of Radiology**, n. 70, p. 312–316, 2009.

MAXIM INTEGRATED PRODUCTS. **MAX1682**. [S.l.], October 2010. Last viewed on 08/01/2016. Available at <http://datasheets.maximintegrated.com/en/ds/MAX1682-MAX1683.pdf>.

NASA. human vestibular system in space. February 2004. Available at: http://www.nasa.gov/audience/forstudents/9-12/features/F$_{H}uman_{V}estibular_{S}ystem_{i}n_{S}pace.html$.

OGAWA, S.; LEE, T. M.; KAY, A. R.; TANK, D. W. Brain magnetic resonance with contrast dependent on blood oxygenation. **Proceeding of the National Acadamy of Sciences USA, Biophysics**, vol. 87, p. 9868–9872, December 1990.

PEASE, R. A. **A comprehensive study of the Howland current pump**. [S.l.], January 2008. Available at <http://www.ti.com/lit/an/snoa474a/snoa474a.pdf>.

QT DOCUMENTATION, QTIMER CLASS. **Qt Documentation QTimer class**. [S.l.], 12 2015. Last viewed on 18.12.2015. Available at <doc.qt.io/qt-5/qtimer.html>.

SMITH, K. fmri 2.0. **Nature**, vol. 484, p. 24–26, 2012.

SOLUTIONS, S. M. **Magnete, Spins und Resonanzen**. [S.l.]: Siemens Medical Solutions, 2003. 224 p.

STEPHAN, T.; DEUTSCHLäNDER, A.; NOLTE, A.; SCHNEIDER, E.; WIESMANN, M.; BRANDT, T.; DIETERICH, M. Functional mri of galvanic vestibular stimulation with alternating currents at different frequencies. **NeuroImage**, vol. 26, p. 721 – 732, 2005.

STEPHAN, T.; HüFNER, K.; BRANDT, T. Stimulus profile and modeling of continuous galvanic vestibular stimulation in functional magnetic resonance imaging. **Annals of the New York Academy of Sciences**, vol. 1164, p. 472 – 275, 2009.

TEXAS INSTRUMENTS INCORPORATED. **TLC2272**. [S.l.], May 2004. Last viewed on 08/01/2016. Available at <http://www.ti.com/lit/ds/symlink/tlc2272.pdf>.

TEXAS INSTRUMENTS INCORPORATED. **MSP430F5359**. [S.l.], October 2013. Last viewed on 14.01.2016.

TEXAS INSTRUMENTS INCORPORATED. **SN74LVC07A**. [S.l.], May 2015. Last viewed on 08/01/2016. Available at <http://www.ti.com/lit/ds/symlink/sn74lvc07a.pdf>.

TYCO ELECTRONICS CORPORATION. **V23079**. [S.l.], July 2015. Last viewed on 08/01/2016. Available at <http://www.farnell.com/datasheets/1918069.pdf>.

WARDMAN, D.; TAYLOR, J.; FITZPATRICK, R. Effects of galvanic vestibular stimulation on human posture and perception while standing. **Journal of Physiology**, n. 551, p. 1033–1042, 2003.

WEISHAUPT, D.; KOECHLI, V. D.; MARINCEK, B. **Wie funktioniert MRI?** 6. ed. [S.l.]: Springer Medizin Verlag Heidelberg, 2009. 172 p.

APPENDIX A – 1

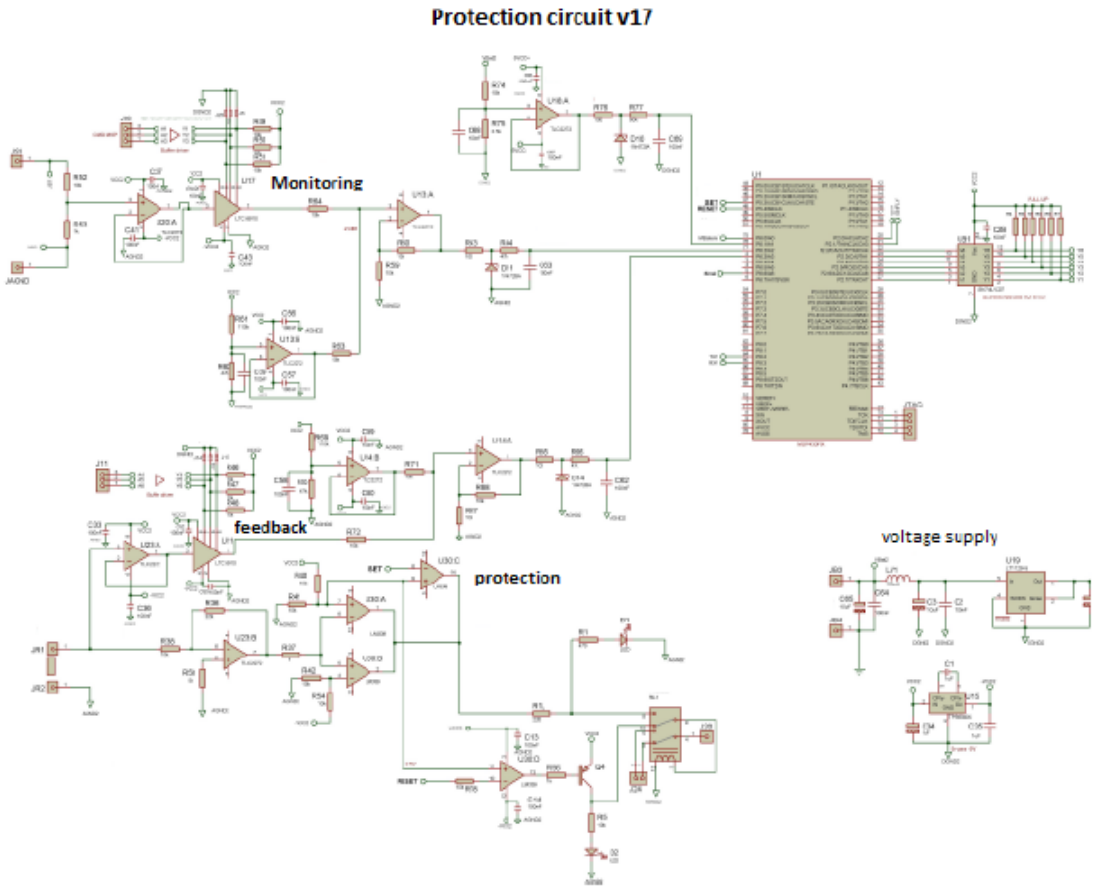

Schematic of the whole GVS circuit - protection circuit

Source: Own authorship

APPENDIX A – 2

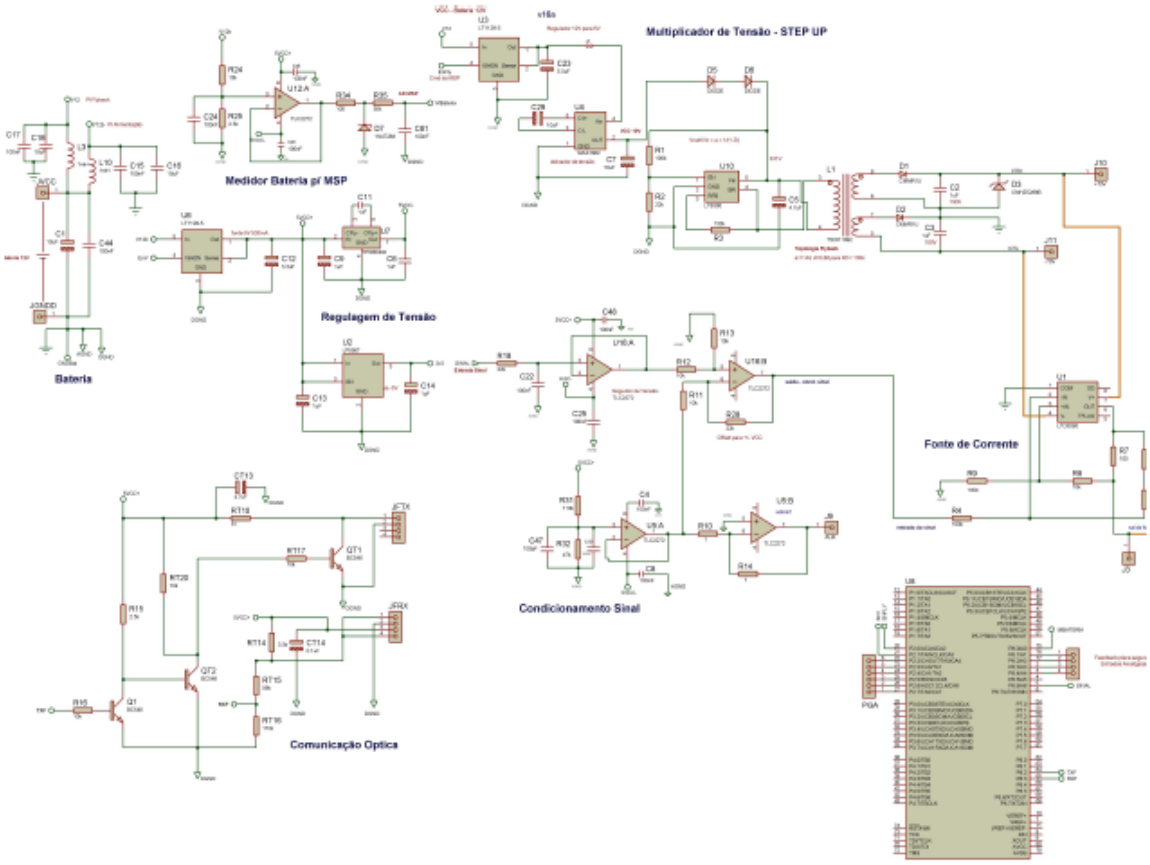

Schematic of the whole GVS circuit - current source circuit

Source: Own authorship

APPENDIX A – 3

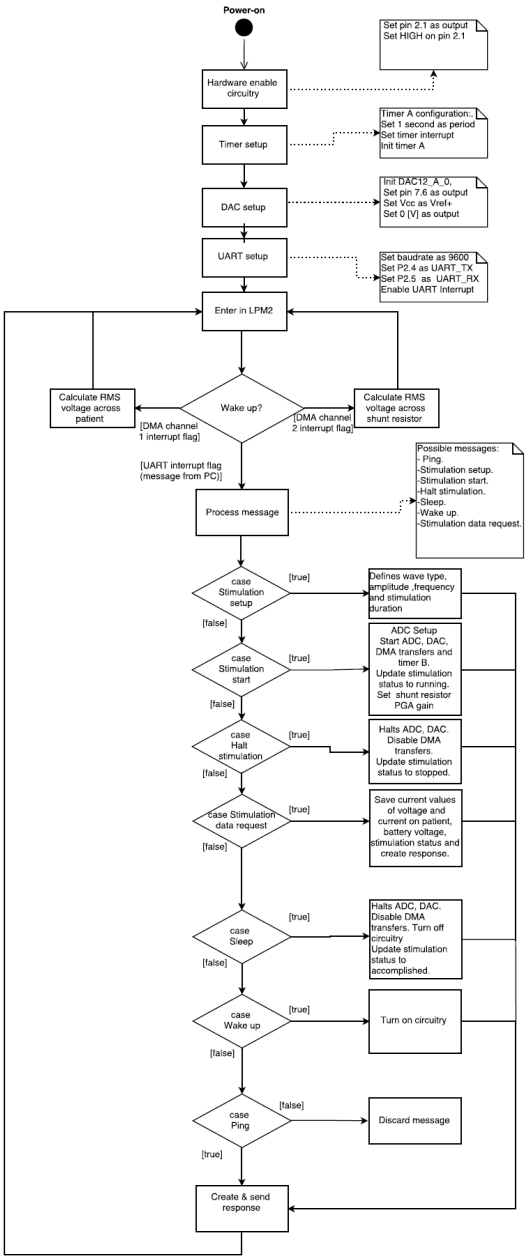

Source: Own authorship

APPENDIX A – 4

Specification of the data communication protocol between PC and MSP for the Galvanic Vestibular Stimulation project – Version 4.3

1 Channel

- Type: Serial communication
- Interface: Optical
- Baud rate: 9600
- No parity
- 1 Stop bit

2 Protocol topology

The protocol implements a master-slave topology where the PC represents the master device, being responsible for initiating the data communication. The MSP does not have the initative to send a frame on its own will. It only sends answers after receiving a frame from the PC, or in other words solicits the stimulation data with the desired frequency during the stimulation process.

3 State machine of the serial communication

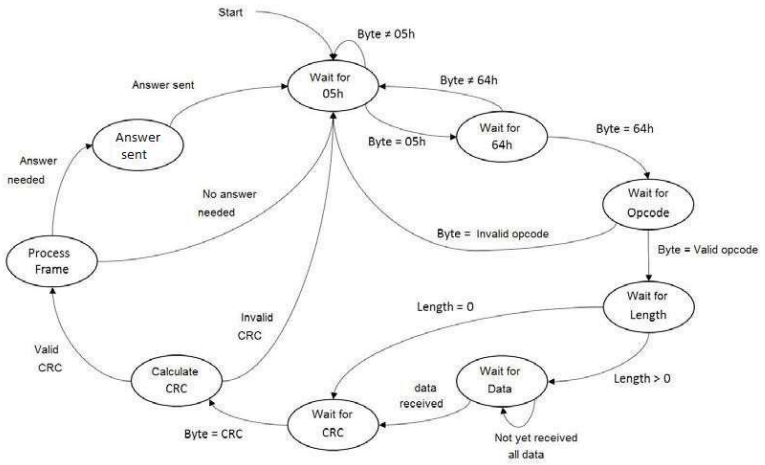

Figure 1: State machine of the serial communication

Obs.: The PC never sends an answert to the MSP.

4 Message opcodes from PC to MSP

Opcode	Description
00h	Ping
01h	Stimulation Setup
02h	Start Stimulation
03h	Halt Stimulation
04h	Sleep
05h	Wake Up
06h	Stimulation Data Request

5 Message layout from PC to MSP

5.1 Ping

SFD	SFD	Opcode	Length	CRC
05h	64h	00h	00h	XXh

5.2 Stimulation Setup

SFD	SFD	Opcode	Length	Data	CRC
05h	64h	01h	05h	XXh XXh ... XXh	XXh

- Data

1. Byte: Stimulation type (0 - Sine; 1 - Quad; 2 - Triang; 3 - const)
2. Byte: Current amplitude on patient
   0 – 0,5 mAp
   1 – 1,0 mAp
   2 – 1,5 mAp
   3 – 2,0 mAp
   4 – 2,5 mAp
   5 – 3,0 mAp
   6 – 3,5 mAp
   7 – 4,0 mAp
3. Byte: Frequency
   0 – 1,0 Hz
   1 – 1,5 Hz
   2 – 2,0 Hz
   3 – 2,5 Hz
   4 – 3,0 Hz
   5 – 3,5 Hz
   6 – 4,0 Hz
   7 – 4,5 Hz
   8 – 5,0 Hz
4. Byte: Minutes of time ON of each stimulation cycle
5. Byte: Seconds of time ON of each stimulation cycle

5.3 Start Stimulation

SFD	SFD	Opcode	Length	CRC
05h	64h	02h	00h	XXh

5.4 Halt Stimulation

SFD	SFD	Opcode	Length	CRC
05h	64h	03h	00h	XXh

5.5 Sleep

SFD	SFD	Opcode	Length	CRC
05h	64h	04h	00h	XXh

5.6 Wakeup

SFD	SFD	Opcode	Length	CRC
05h	64h	05h	00h	XXh

5.7 Stimulation Data Request

SFD	SFD	Opcode	Length	CRC
05h	64h	06h	00h	XXh

6 Message opcodes from MSP to PC

Opcode	Description
20h	Ping answer
21h	Stimulation Ready - Answer to Stimulation Setup
22h	Stimulation Started - Answer to Start Stimulation
23h	Stimulation Halted - Answer to Halt Stimulation
24h	Sleeping - Answer to Sleep
25h	Awaken - Answer to Wake Up
26h	Stimulation Data - Answer to Stimulation Data Request

6.1 Ping answer

SFD	SFD	Opcode	Length	CRC
05h	64h	20h	00h	XXh

6.2 Stimulation Ready

SFD	SFD	Opcode	Length	CRC
05h	64h	21h	00h	XXh

6.3 Stimulation Started

SFD	SFD	Opcode	Length	CRC
05h	64h	22h	00h	XXh

6.4 Stimulation Halted

SFD	SFD	Opcode	Length	CRC
05h	64h	23h	00h	XXh

6.5 Sleeping

SFD	SFD	Opcode	Length	CRC
05h	64h	24h	00h	XXh

6.6 Awaken

SFD	SFD	Opcode	Length	CRC
05h	64h	25h	00h	XXh

6.7 Stimulation Data Request

SFD	SFD	Opcode	Length	Data	CRC
05h	64h	26h	05h	XXh XXh ... XXh	XXh

- Data

1. Byte: Stimulation status (0 - running; 1 - accomplished; 2 - stimulation stopped by patient; 3 - stimulation stopped by overcurrent)
2. Byte: Current amplitude in hundreds of µA (Ex: 35 in the protocol = 3,5 mAp)
3. Byte: Voltage amplitude in Volts (Ex: 32 in the protocol = 32 Vp on patient)
4. Byte: Current frequency in hundreds of mHz (Ex: 75 in the protocol = 7,5 Hz)
5. Byte: Battery 1 level in hundreds of mV (Ex: 29 in the protocol = 2,9 V)
6. Byte: Battery 2 level in hundreds of mV (Ex: 18 in the protocol = 1,8 V)
7. Byte: Stimulation status (0 - idle/without current applied to patient; 1 - with current)

7 CRC

The CRC is the result of the byte wise XOR operation of opcode, length and the data bytes.

Source: Own authorship